Doty, F. David

High-Throughput RF Coils for High-Field MRI

Abstract

Improvements in signal to noise ratio (SNR) and ease of use of magnetic resonance imaging (MRI) rf coils are needed to improve image quality and patient throughput in high-field MRI. The goal of this Phase II project is to continue the development of novel rf coil topologies and rf balancing circuits that have demonstrated substantially improved technical performance, reduced cost, and greatly simplified tuning procedures. The success of the Phase I effort demonstrated the unique contributions possible with our advanced, proprietary, simulation software and patented coil technology. The circular polarization (CP) coils built and tested during Phase I demonstrated an improvement of a factor of 3 to 15 (depending on the reference CP technology) in tunability (ability to tune and match efficiently over a wide range of sample loading conditions at very high fields) for equivalent B_1 homogeneity. Also, much higher B_1 homogeneity is maintained over the full range of load conditions. Significant improvements were also achieved in SNR and passive B_0 shimming, and further gains are expected here during Phase II. We denote these coils "litzcages", as they embody both paralleled conductor elements with insulated crossovers similar to that in our prior "litz coil" technology and capacitively segmented phase shifts and four-point drive to achieve highly stable circular polarization.

We have demonstrated feasibility of a quadrature, single-tuned, semi-open, passively shimmed rf litzcage with an axially asymmetric field profile. The Phase I saw the development and bench testing of numerous linear and CP litz coils, including one for human knee studies at 3 to 6 T, two for small-animal research at 470 MHz, one for single-resonance human head MRI at 2 to 4.2 T, and one for double-resonance human head MRI at 1.5 T.

Field testing of a 3 T ^{1}H head coil will begin early in Phase II at the Hershey Medical Center, Hershey, PA, followed by final produtizing and initial FDA approval procedures. The Phase II will continue model optimizations and development and field testing of CP single-resonance litzcages for knee, neck, and torso at 3-7 T, as well as smaller CP litzcages for animal research at the highest fields. Preliminary development of a 3 T double-resonance multinuclear ^{1}H/X head coil utilizing our linear litz coils is also planned. The primary objectives are to permit a substantial increase in MRI patient throughput (thereby reducing scan costs) via relatively inexpensive upgrades of head, knee, neck, and torso rf coils in existing high-field MRI scanners, and/or to enable the more detailed diagnostic studies that are currently not practical because image acquisition time would be excessive.

Key Words:
MRI, brain, rf coils, birdcage, high-field

Business/market potential:

There are over 13,000 MRI systems installed world-wide, and annual MRI equipment sales are currently ~$3B. The proposed rf coils would permit substantially reduced imaging time (hence, cost) and reduced patient distress for head imaging in most high-field MRI scanners above 1.5 T at relatively modest upgrade costs. Total upgrade market potential over the decade following completion of the Phase II exceeds $40M.

High-Throughput RF Coils for High-Field MRI

1.0 Phase II Specific Aims

The goal of this project is to enable a new level of clinical performance in MRI by continuing the development of a novel rf coil topology and rf balancing network that substantially improves technical performance, reduces cost, and greatly simplifies tuning procedures. The coils will be compatible with the requirements for clinical high-field MRI, especially functional MRI (fMRI), head microscopy, and whole-body MRI at 3 T and higher. During Phase I, we demonstrated feasibility of a quadrature, single-tuned, semi-open, passively shimmed rf litzcage for human head with an axially asymmetric field profile. This novel coil features major tuning simplifications and improved robustness compared to conventional birdcages [*1, 2*] or Transverse Electric/Magnetic (TEM) resonators [*3, 4*] and improved versatility and patient compliance. The highly effective but semi-open rf shield structure reduces radiation losses by nearly two orders of magnitude compared to the unshielded birdcage [*5*] while maintaining maximum access and openness [*6*].

Much higher B_1 homogeneity is maintained over the full range of load conditions, which contributes to improved signal to noise ratio (S/N or SNR). Both light-load (small patient) and heavy load (largest patient) SNR are expected to exceed that of state-of-the-art head birdcages by ~2 dB, equivalent to a 30% reduction in image acquisition time. Mid-range-load SNR may be improved by ~1.5 dB. The approach appears to be advantageous for most applications from mid-field up to the highest fields and largest sample sizes, including whole-body coils for 3 - 4 T. The Phase I objectives (greatly improved load range, openness, passive shimming, and the potential for reduced cost and increased patient throughput) were met in a demonstration head coil at both 128 MHz and 180 MHz. Additional experiments were performed to demonstrate the potential of the 4-point-drive litzcage in knee and whole-body coils at 3 T as well as in coils for small-animal research at 200-750 MHz.

Field testing of a 3 T ^{1}H head coil and a 3 T knee coil will begin very early in Phase II at the Hershey Medical Center, Hershey, PA, and field testing of a 3 T torso coil and a double-tuned ^{1}H/X head coil are planned for the second year. The Phase II will continue with the development and field testing of quadrature litzcages optimized for human head, knee, neck, torso, and wrist at 3 to 7 T, as well as smaller litzcages for animal research at the highest fields. The FDA approval process for head, knee, and neck coils will also begin during the Phase II.

The overall Phase II objective is to permit a substantial increase in MRI patient throughput (thereby reducing scan costs) via relatively inexpensive upgrades of robust knee, head, torso, neck, and wrist rf coils with greatly reduced tune-up time in existing high-field MRI scanners. The Phase II includes the following specific aims:

1. Field-test and productize the 4-point-drive CP semi-open litzcage RF coil for human head MRI at 3 T.
2. Improve designs of passive shims (especially Z^3, X^2-Y^2, and Y^3) that are compatible with the rf-coil shield space for corrections of B_0 within the human head.
3. Improve circuit models for accurately predicting parasitic inhomogeneous modes near the homogeneous resonance in large, tunable, circular polarization (CP) MRI volume coils with 4-point-drive networks at high fields.
4. Validate the improved models in lower-cost higher-performance human knee, neck, and torso prototype coils for clinical applications at 3 T and in rf coils for small-animal research at 200-750 MHz.
5. Obtain FDA approval of 4-point-drive CP litzcage coils for human head, knee, and neck at 3 T.
6. Develop improved bench test methods for accurately mapping B_1 homogeneity in large, high-field MRI coils.
7. Develop an improved understanding of the relationship between the current distribution near the ends of a CP MRI volume coil and the losses outside the region of interest (ROI).
8. Explore the possibility of manipulating the external E field in novel ways so as to oppose $\partial\mathbf{A}/\partial t$ within the ROI and thereby reduce sample losses below what has generally been thought to be theoretical limits.

2.0 Context and Significance of the Proposed Effort

It is hard to imagine a medical diagnostic technique that has received more attention and intensity of R&D during the past two decades than MRI. By many, it is seen as epitomizing the objectives of basic and applied scientific research. Yet, in spite of this and the fact that MRI equipment sales last year were ~3 billion dollars, some will argue that its real diagnostic contributions are often marginal when viewed objectively by outcomes. There are several reasons for the continuing perception by some that MRI often shows limited diagnostic value, but the problem is usually limited image resolution or high cost [*1*]. (Gradient acoustic noise, which may exceed 115 dB_A, from the rapid scan protocols is also sometimes a significant concern in MRI [*7, 8*].) Brain scans at magnetic field B_0 of 1.5 T typically obtain transverse resolution of ~1 mm for a 5 mm slice thickness (equivalent to 1.7 mm isotropic resolution) in about 5 minutes. Of course, cost is primarily related to patient throughput, and image acquisition time generally increases as the ***sixth power*** of the reciprocal of the isotropic resolution and is inversely proportional to the square of SNR. Except for very small coils, SNR usually increases linearly with B_0 (for a constant voxel size, sample size, and rf coil design) [*2*], but it is highly dependent on the details of the rf coil design.

Rf coil design over the past two decades has been based primarily on simplified relationships with restricted ranges of applicability. Recently, full-wave numerical solutions of specific designs have become possible [*9*], but there is still no assurance that an optimum design has been obtained [*2*], even for a specific set of conditions. However, a method of determining ultimate achievable S/N for specific conditions has recently been published [*10*].

Actually, resolution in MRI is always limited by contrast-to-noise ratio (CNR), not SNR. Naturally, a large array of contrast enhancing agents and techniques especially for high-field MRI have been developed over the past two decades. However, composite CNR is always proportional to SNR, wherein most of the coil-dependence resides. Since T1 (longitudinal relaxation time) increases and T2 (transverse relaxation time) decreases with field, high fields have often shown disappointing improvements in CNR, SNR, and resolution. These disappointments have often been exacerbated by poorly optimized rf coils.

If the coil's S/N can be increased by 30%, the benefit is equivalent to increasing the polarizing magnetic field B_0 from 1.5 T to 2 T, which would typically cost over $500K in a new scanner and is not an option for installed scanners. We, like many others, believe rf coil optimization still offers the most overall potential for gains in MRI system performance per cost.

For the past 15 years, it has been generally believed that circular polarization (quadrature reception) is always superior to linear polarization (or at least when sample losses dominate) and that the quadrature birdcage was the ultimate coil design for cylindrically symmetric samples [*11, 12*]. We have recently demonstrated higher performance (in S/N, B_1 homogeneity, and especially in ease of use) with a radically different approach to linear coil design over a wide range of conditions [*13*]. **Figure 1** shows results from one particular case from Hershey Medical Center. This group of distinguished coil experts (C. Collins, M. Smith, Q. Yang, et al) has been unable to obtain or fabricate in-house an adequately functioning CP birdcage for the knee at 3 T (the knee coil seems much more challenging than the head coil, as loading changes by a much greater factor for various sample positions and subject weights). They have successfully built a number of linear knee birdcages, so our comparisons here were to the best of their linear knee birdcages.

Figure 1. MRI of human knee at 3 T obtained in a Doty linear rf litz coil. Hershey Medical Center, PA.

While B_1 homogeneity and S/N were both better than obtained on their best birdcage, the researchers agreed that the most important advantage of our coil was that it could be tuned and matched within seconds to loads varying by more than an order of magnitude. Our linear litz coil was ~20% more efficient (in power required for a given pulse width) and its region of homogeneous rf field was also ~20% longer, so normalized efficiency appears to have been ~40% higher, which is a little better than expected from our comparative simulations.

We also recently obtained excellent data at the other end of the size spectrum. We compared a *linear* litz coil of 19 mm diameter and 18 mm homogeneous rf length, developed during the Phase I for mouse brain research, with a well optimized *quadrature* birdcage built by an experienced small-animal imaging team at Washington University (J. Ackerman, J. Garbow, and S.-K. Song) at 200 MHz for MRI in a horizontal-bore magnet. (In spite of the small dimensions, this is still a sample-dominated case [the loaded Q is ~120, a little less than half the unloaded Q], because the relatively large shield diameter allows the coil to achieve exceptionally high magnetic filling factor.) Our linear litz coil achieved ~15% higher S/N than the quadrature birdcage (which was about 5% larger in diameter and ~5% shorter). More significantly, the B_1 homogeneity of the litz coil appeared to be significantly better and it could be tuned and matched in seconds to any sample over a wide range of frequencies. The importance of this latter attribute should not be underestimated. It reflects a marked advantage over birdcage and related coil designs. Figure 2 shows a single brain slice (in-plane resolution of 175 microns with a slice thickness of 1 mm) from a T2-weighted, multi-slice experiment on a live mouse.

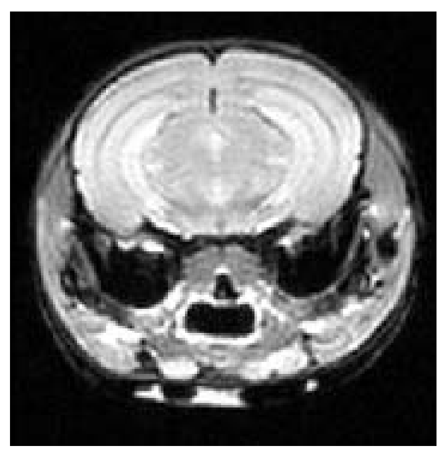

Figure 2. Live mouse brain at 4.7 T, linear litz coil (Biomedical MR Laboratory, Washington University).

Certainly, conventional birdcages (both shielded and unshielded) and TEM resonators with end rf mirrors have performed quite well for human head MRI, where the small volume of the brain relative to the coil's volume makes stable tuning quite practical. However, S/N suffers a little due to the increased size required for adequate tunability in a high-field coil utilizing loose couplings between elements – partially because both radiation losses and sample losses outside the ROI will also increase. These losses are extremely important at high fields [*14*].

The approach we have shown to be decidedly superior in linear coils is to use tightly coupled elements and to force an optimal surface current distribution using a "woven" pattern of parallel foil conductors with insulated cross-overs [*13*] in a way to improve rf flux transparency and Q. We have called these coils "Litz coils" [*15, 16*]. These linear litz coils have consistently demonstrated improved S/N, B_1 homogeneity, and ease of use under sample-dominated conditions compared to any other linear rf coil under both single and double-resonance conditions.

The numerical simulations and bench tests on the quadrature litzcages developed during Phase I suggest that with conventional (static) matching networks the S/N gain with our litzcages may be quite modest (~10%) for the median human head compared to current state-of-the-art semi-open coils, though the gains for very large and very small patients will be greater. However, the ease with which our coil can be tuned and matched without degrading B_1 homogeneity now makes dynamic tuning and impedance matching practical [*17*], which offers additional benefits.

Optimum noise match to a low-noise preamp requires a rather high VSWR (the voltage standing wave ratio often needs to be greater than 4 [*18*]), but the transmitter must be impedance matched to the coil, typically with VSWR less than 1.5. This is generally accomplished by designing the preamp with an input impedance of 100-500 Ω so that it obtains best noise figure (NF) from a source impedance of ~50 Ω. The coil is then matched reactively to 50 Ω for the transmitter's requirements. What appears to not be generally appreciated is the deleterious effect of the switched load (because the matching elements are reactive) on both B_1 homogeneity and channel isolation (which affects S/N) in the coil. While our four-point drive method in itself reduces these effects by a factor of 2-3, the tuning range and stability of our network also allows us to consider adding dynamic tuning (using varactor diodes) to fully mitigate these affects.

The contribution of our Phase I developments to MRI RF coil technology now appears likely to be especially significant for high-field knee and whole-body, primarily because they are more demanding technically, owing to the much wider range of loading conditions that are encountered there. High-homogeneity CP coils for knee and torso applications at 3 T and higher do not appear to be available yet – at least from third-party sources. So it appears that a robust, quadrature, high-homogeneity, easily tunable coil for knee or torso applications at the highest fields would represent a very significant contribution to clinical and research MRI instrumentation.

Both delivery problems and the relatively high costs (~$22K to ~$60K) of MRI rf coils from the major vendors have led to several coil-company start-ups over the past several years, but it is clear that there is still a real need for better coils for many experiments and clinical applications.

A major goal of this Phase II project is to see how close we can come now to theoretical S/N limits in large, high-field quadrature coils where sample losses strongly dominate. The novel quadrature litzcages developed during the Phase I (and covered in our pioneering patent, [*15*]) are expected to enable major throughput advantages in many applications, especially since the recent enhancements in our software have enabled us to improve our coil optimizations and give us confidence that the global optimum is found.

3.0 Phase I Final Report: Advances in MRI RF Coil Technology

Grant 1 43 CA91455-01 (RR GM ZRG1 SSS-7)

Dates: Apr 1 through Nov 30, 2001. Site: Doty Scientific, Inc., Columbia SC

Primary Technical Staff	Role	Dates	Approx. Total Hours
F. David Doty, Ph.D.	Principal Investigator	4/1-11/30	500
George Entzminger	Electrical Engineer	5/1-11/30	400
Zubaid Rafique	Computer/Electrical Engr.	6/15-11/30	600
John Staab	Electrical Engineer	5/1-11/30	100
Tod Welsh	Electrical/Mechanical Engr.	8/20-11/30	150
Scott Deese	Chemical Engr./Draftsman	6/1-9/30	200
Jerry Hacker	Machinist/Shop Manager	5/1-10/30	150

Summary of Phase I specific aims: (1) Greatly improved load range, openness, and robustness of the high-field MRI rf head coil; (2) Developments in passive shimming for improved image quality; (3) Substantial potential for reduced production cost and increased patient throughput from reduced tune-up time and improved SNR.

3.1 Brief Synopsis of Current MRI RF Coil Technology

3.11 Birdcages. For more than a decade, the birdcage coil (see **Figure 3**) has usually been chosen for MRI [*6, 19, 20*] because of its ability to achieve circular polarization with high homogeneity under symmetric conditions, but the TEM resonator (shown in **Figure 4**) has recently gained popularity because it has often performed better with large samples at very high fields [*3*]. It has been shown that the first-order quadrature and balancing errors in the birdcage can be corrected with just two judiciously placed correction capacitors [*19*]. While this has been effective in compensating for manufacturing tolerances in smaller coils or at low fields (where sample-dependent shifts and asymmetries are small), it is not a satisfactory method of correcting sample-dependent asymmetries or higher-order errors, which become quite important as high-field-magnet costs impose more severe constraints on coil space.

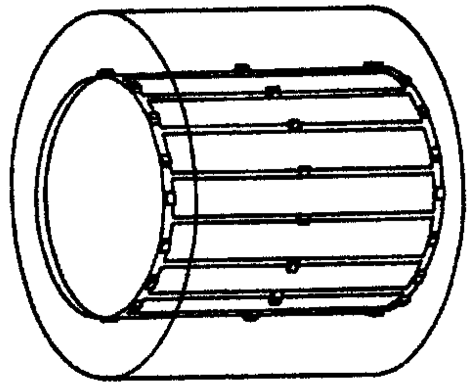

Figure 3. The hybrid birdcage coil as normally depicted – sans coupling circuits.

3.12 TEM Coils. The error-correction problem is even more severe in TEM resonators, as coupling coefficients between elements are much weaker. As a result, TEM resonators must be more fully shielded (the end rf mirror is often essential for satisfactory tuning stability). Published data showing the SNR advantage of the TEM resonator compared to the birdcage in a number of high-field cases [*3*] have been disputed by some distinguished MRI coil experts (B. Edelstein, R. Hurd, J. Tropp, etc.). They indicate several of the flaws in the comparisons were that the reference birdcages lacked end mirrors and were otherwise not fully optimized for the loads [*21*]. Recent simulations in-house (and by others) during the Phase I call into question the argument that the TEM coil's reduced inductance and radiation significantly improve SNR in the absence of the end mirror, which impairs patient access. Also, recently published experimental comparisons indicate that the TEM head coil at 3 T is actually slightly less efficient than a fully comparable and properly optimized birdcage [*22*].

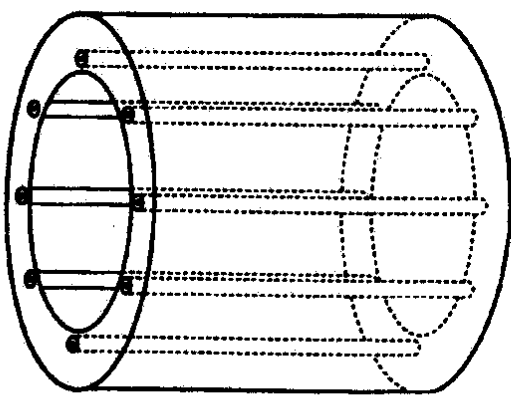

Figure 4. In the TEM resonator, the end ring currents are mostly replaced by increased shield currents.

An undeniable characteristic of this useful coil (which is just one of the enormous contributions of friend Tommy Vaughan) is that the much weaker couplings between elements make it more difficult to avoid mode splitting and maintain symmetric tuning to the homogeneous mode [*23*]. Moreover, the theoretical calculations and "experimental images show, for the TEM, a dramatically larger sensitivity to perturbation than for the birdcage" because of mixing with the nearby inhomogeneous modes [*23*].

3.13 Local Coils. Surface coils and arrays of surface coils (phased arrays) offer improved SNR from regions near the surface but at considerable cost in B_1 homogeneity and usually substantial loss in SNR from deeper regions. With phased arrays [24], it is possible to achieve some signal gain even for deep tissue in localized regions compared to an optimized, short volume coil; hence, they are often used for specific studies. However, volume coils remain the work-horse coil for general imaging.

3.14 DotyNMR Linear Litz Coils. We devote a little more space here to reviewing our linear litz coils [*15*], as they are not yet well known to most MRI coil researchers. They served as the prelude to this Phase I CP Litzcage effort and are still the best option for a wide range of MRI applications, especially for double-resonance. One of the projects in the proposed Phase II effort will be the development of a 3 T double-resonance head coil utilizing our latest linear litz coils, as discussed later.

Our initial conceptual design approach was to explore coils related to the Alderman-Grant resonator [*25*], where the current distribution (hence, inhomogeneity) was essentially independent of capacitor matching and phase shifts, as this appeared to be the most practical route to tuning simplifications with variable loads. We were quite surprised to find the calculated magnetic filling factor η_F for birdcages was often below 6%, while η_F for the Alderman-Grant resonator with the Kost 90^0 window optimization [*26*] was often comparable (even after dividing by two to correct for the difference between circular and linear polarization), and (loaded) Q_L for small frequency-diameter products (*fd*) was generally higher. Experiments confirmed the numerical calculations [*13*].

The B_1 rms inhomogeneity σ_B of the Kost-optimized Alderman-Grant (KAG) resonator with a large sample was found to be 9.5%, which is slightly better than that of the 8-rung BHP (balanced high-pass) birdcage with a close shield when typical sample-dependent effects on coupling and tuning asymmetries are included [*13*]. Also, the $\eta_F Q_L$ product (i.e., S/N) of the KAG coil is generally higher for *fd* below 8 MHz-m. Since this coil is much easier to tune, it is not surprising that it (or a close relative) continues to be the resonator of choice in probably 95% of high-field spectroscopy applications for *fd* in the range of 3-8 MHz-m. One drawback of the KAG coil is that it lacks transverse transparency so it cannot be used effectively with an orthogonal coil or circular-polarization.

The homogeneity limitation of the slotted resonator and related coils comes from the tendency of the current to concentrate near the edges of the flux-windows. However, this behavior can be controlled from the use of parallel foil conductors with insulated cross-overs that force the current to re-distribute in a more optimal manner. The rf current will take the low-inductance route unless forced otherwise. So we developed efficient software *COILS* to simulate this current distribution problem and explored a large number of novel patterns which improved $\eta_F Q_L$ and σ_B by a substantial amount compared to prior coils, including ideal linear birdcages. One such pattern is depicted in **Figure 5** and can be understood by referring to previous publications of related litz coils [*13*]. We will return to the Phase I linear litz coil developments later in discussions of double-resonance coils for Phase II, but the primary focus of the Phase I effort was the CP litzcage.

Figure 5. The CFL2 linear Litz coil.

3.2 The CP Litzcage

Field simulations show that even with perfect symmetry, at least 12 rungs are required for adequate B_1 homogeneity (for most purposes) in a closely shielded conventional birdcage with a relatively large ROI (>0.7*d*). However, our rf circuit model shows that the 8-section birdcage is about twice as robust (tunable and correctable) as the 12-section birdcage because it is possible to attach two adjustment variables to nodes at 45^0 with respect to the feed planes, which simplifies the symmetrization problem when tuning to different loads. While the 45^0 nodes are available in the 16-section birdcage, it has twice as many distinct capacitors and hence half the tuning range. Symmetrization adjustment in the 12-rung birdcage, on the other hand, tends to mix asymmetrically with all tune and match adjustments, which complicates the process.

Our basic "litz" concept of using parallel conductors with judiciously placed insulated crossovers may be applied to the conventional 8-rung CP birdcage to make it much easier to obtain high B_1 homogeneity and greatly increased tuning range, as will become clear in the following sections. The resulting coil has homogeneity and S/N comparable to that of the ideal 16-rung birdcage (supporting simulations are presented in section 4.3) while retaining the tuning robustness of the 8-rung birdcage. The complete solution requires a 4-point-drive network as well.

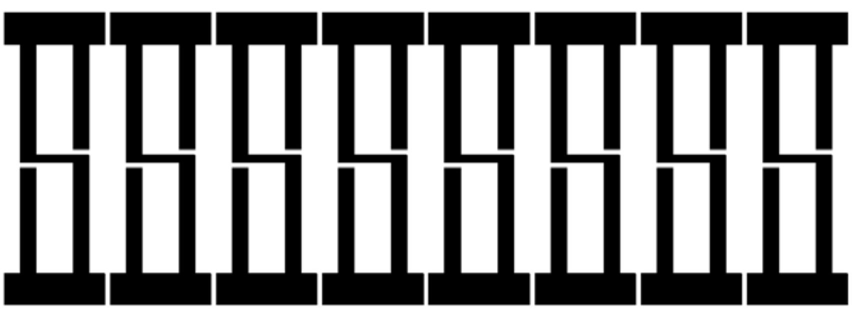

Figure 6. One surface of the High-pass Litzcage foil pattern. The other surface completes the central crossovers.

Figure 6 illustrates the primary surface of our standard 8-section high-pass litzcage pattern, laid out flat. Each rung in the 8-section birdcage has been replaced by two parallel rungs with an insulated crossover at the center; so it has 16 rungs, but only 8 sections. From the axial symmetry, each of the two parallel rungs per section must carry equal current, irrespective of the section's relative phase. From an rf circuit perspective, the homogeneous mode is almost indistinguishable from that of Crozier's parallel-rung 8-section birdcage [*27*], which is of course quite similar to the conventional birdcage from an rf perspective. However, we will show that the addition of the insulated crossovers in each section gives a dramatic improvement in B_1 homogeneity. Moreover, the 30% reduction in stray capacitance in the litzcage compared to the 8-rung birdcage allows it to tune ~20% higher.

More than 8 rungs have been used (even 24) in birdcages for reasons other than to improve homogeneity near the edges in the central plane – it has made it easier to tune reliably to higher frequencies, partially because accurate models for the hybrid birdcage have not been reported. It appears that with our litzcage there is no longer a need for more than eight azimuthal sections, even at the highest fields.

3.3 Improvements in Tuning Range/robustness and B_1 Homogeneity in CP Coils

The data will show that our novel combination of three features (4-point balanced drive with orthogonal symmetrization, the 8-section litzcage, and zero-center variable capacitors) developed during the Phase I has increased the tuning range of homogeneous CP MRI coils by an order of magnitude compared to standard methods. Still, the maximum tuning range is only ~8%. In cases like human knee and torso coils and high-field small-animal coils, the sample-induced tuning shift from a large load can exceed 4%, so it seems that the absence of any one of the mentioned tuning-range-enhancing features would result in a coil with less tuning range than often needed.

Most commercial coils appear to lack all three of these features, which leaves a tuning range of less than 1% with good homogeneity and channel separation for the standard 12-rung birdcage. The variation in the loading among human adult heads is rather small, so it is not too difficult to accommodate the normal range of head loads (at least below 3 T) by simply increasing the coil ID to 28 cm – a little more than needed for the largest head. However, the desire to have increased coil openness for improved access seems incompatible with preliminary tune-up outside the magnet without increased tuning range, as increased openness increases coil interaction with the surroundings. Also, it is often desirable to incorporate surface coils for improved local reception. The tuning and homogeneity perturbations associated therewith are generally difficult to deal with in high-field birdcages with 2-point drive.

When coils are used for both transmit and receive, the tune/match conditions should change between these two conditions. The coil should be matched fairly close to the amplifier impedance (50 Ω) during the transmit pulse for stable and reliable amplifier operation. However, during receive, a high VSWR is *required* for optimum SNR. While this has been understood theoretically for at least 3 decades, to our knowledge, this has not previously been properly addressed in CP coils, as it requires dynamic compensating changes in both the tune and the match controls, and such changes risk significant degradation of B_1 homogeneity with conventional birdcage tuning methods.

We note that most research MRI on animals is performed in smaller magnets, where space is even more of a premium. There, it is not uncommon to need to study objects that fill 60-85% of the coil's ID and may extend out both ends. Our experience and simulations indicate it is impossible to achieve high B_1 homogeneity over such a range of conditions (even for a 10 cm coil at only 200 MHz) without the full capability of our 4-point-drive litzcage.

Finally, the most challenging case is certainly whole-body coils at high fields. Here one must deal with (a) the widest range of sample loading conditions (juveniles to large adults), (b) the full range of patient positioning possibilities, (c) the frequent need for compatibility with surface coils (including active detuning) and other support hardware, and (d) stringent B_1 homogeneity requirements because of its link to localized Specific Absorption Rate (SAR). Since sample loading generally increases quadratically with sample volume, it seems that high-field whole-body rf coils must be of the band-pass (hybrid) type to minimize dielectric loading, at least for torso imaging. This reduces the tuning range by nearly a factor of two and introduces additional inhomogeneous modes closer to the homogeneous mode. Not surprisingly, current options for whole-body rf coils for 3 T and above are generally unsatisfactory for many applications. Hence, we have devoted considerable effort to coil models appropriately scaled to approximate the tuning conditions of the high-field whole-body band-pass litzcage. Here the advantages (in ease of tuning, improved B_1 homogeneity, and SNR) of our 4-point drive network and the 8-section litzcage are most important.

3.4 Development of Accurate RF Circuit Models for High-Field CP Coils

3.41 Need for More-complete RF Circuit Models. Even though birdcages of countless varieties have been in wide usage for sixteen years, published circuit models leave much to be desired. The major source of the problems is that to make the models analytically tractable, it has been customary to either ignore or use highly simplified expressions for most of the couplings (electric and magnetic), circuit losses, and propagation effects.

The standard (simplified) theoretical model (ignoring all mutual inductances and stray capacitances) gives the following for the modes of the balanced high-pass birdcage [*28*]:

$$\omega_m = \left[C\left(L_E + 2L_{TRL} \sin^2 \frac{\pi m}{N} \right) \right]^{-1/2} \tag{1}$$

where L_E is the end ring (section) inductance and L_{TRL} is the rung inductance.

The highest mode, m=0, also known as the end-ring mode, has zero current in the rungs. The next-highest mode, m=1, is the homogeneous (NMR/MRI-useful) mode. The above equation is typically off by more than 15% for the homogeneous mode and even more for the other modes. For a typical unshielded 16-rung birdcage, the above gives $f_2 \approx 0.57 f_1$, while a more complex model gives $f_2 \approx 0.67 f_1$ [*26*]. For an 8-section birdcage inside a full cylindrical shield with shield/coil diameter ratio *s* of 1.4, we typically find $f_2 \approx 0.79 f_1$, while equation (1) predicts $f_2 \approx 0.68 f_1$ (for L_{TRL} = 36 nH and L_E =12 nH). Moreover, another weak mode m_{2+} sometimes appears a little above f_2 (which is usually split) and another weak mode m_{1+} usually appears a little above f_1, neither of which are predicted by either eq. (1) or the more complex published models but are generally captured by our models.

Publicly available software uses somewhat better birdcage circuit models and can allow prediction of capacitor values within ~3% for low-pass birdcages at small *fd* products. However, for midrange high-pass birdcages the errors are typically twice this large, and errors of 15% are not uncommon. For the high-range band-pass birdcage, the errors are generally over 20%. Clearly, both the analytical and the available software models leave much to be desired.

For two-point capacitor-only quadrature drive, the capacitor accuracies required to place the resonance within one-half of the maximum tuning range (the range which keeps the loaded peak-to-peak relative rung current errors below 15%) are extremely tight. Our simulations indicate the following mean-capacitor-value accuracies are required: for a 16-rung (unbalanced) low-range low-pass birdcage, the capacitors must be within 1.5%; for a 16-rung (balanced) high pass birdcage, they must be within 0.8%; for a 16-rung high-range hybrid birdcage, they must be within ~0.4%. Indeed, it is difficult to measure small capacitors (~5 pF) within better than 1.5%, even at low frequencies.

We note that the above numbers are not at odds with other's published results. For example, Tropp showed that a single capacitor error of up to 8% in a 16-rung low-range low-pass birdcage could be corrected by two suitably positioned corrections, but this does not address the problem of mean rung error, which is more critical by a factor of up to $n/2$ (depending on Q), where n is the number of distinct capacitors in the coil.

Another justification for a more accurate rf circuit model is to test some of the predictions from simplified analytical models, which often seem to be in conflict with experimental data. The analytical theory for the correction of the perturbed low-pass birdcage [*19, 29*] includes the following assumptions (in the order we think of greatest concern): (1) zero mean errors; (2) no mutual inductance between rungs; (3) no input/output matching network; (4) lossless sample and circuit elements; (5) zero ring inductance; and (6) no stray capacitance. One of the conclusions of this simplified theory which we believe to be invalid is that a suitable measure of the symmetry (hence, rung current errors and B_1 homogeneity) of the coil is the fractional splitting of the two homogeneous modes. A subsequent conclusion is that the worst-case cross-talk in a perturbed birdcage is given simply by -20 log ξQ, where ξ is the relative mode splitting; and the coil may be considered corrected when ξQ is reduced below a fixed target value. Another simplified derivation suggests the maximum relative field inhomogeneity within 70% of the coil diameter is only seven times the relative frequency shift in the fundamental mode induced by a major perturbation [*28*]. Finally, the conclusions of the simplified perturbation theory for the low-pass birdcage have been applied in the published literature without proof to the high-pass and band-pass birdcages.

Our simulations, numerous experiments, and other recent analyses conflict with the above conclusions. For example, it has recently been shown that the inhomogeneity of a perturbed coil improves as the distance to the nearest inhomogeneous mode increases [*23*]; but the mode structure is known to depend on the mutual coupling coefficients [*23, 28*], which are ignored in the perturbation theory. Our experiments and models, whether simple or complex, consistently show that perturbations along a feed plane have almost no effect on cross-talk (as long as the two modes are at the same frequency) *but still perturb homogeneity* almost as severely as the perturbations in planes 45^0 with respect to the feed planes, contrary to the predictions based on first-order perturbation theory. So the inhomogeneity of a perturbed coil cannot be assessed simply from cross-talk or the relative magnitude of a single perturbation.

Channel isolation is much more sensitive to off-axis errors than is σ_B. As noted above and predicted from first-order theory [*19*], modest single-rung errors (up to 8%) with a proper correction are acceptable from a B_1 homogeneity perspective when the sample diameter is less than ~70% of the coil diameter. Of course, the errors are seldom limited to a single component; but even more challenging is dealing with the discrepancy between the effects on channel isolation predicted from simplified theories and the real effects seen both in experiments and in the more complex circuit models. While channel isolation may not need to be better than ~15 dB for nearly optimum SNR, isolation is probably the simplest test by which the user can check coil symmetry on the bench. For this test to have a useful correlation with σ_B, our simulations show total off-axis reactance errors need to be below ~1.5% *prior* to correction.

It is true that the series matching reactance is large compared to the reactance of the rung's stray (or transmission-line) capacitance for the low-frequency examples (e.g., a 24 MHz unloaded small head coil) used to illustrate the analytical models so superbly developed by Tropp and others [*5*, *11*, 19], and for this condition the coupling capacitors have negligible effect on channel isolation and generate acceptably small symmetry perturbations. This is not the case though for the loaded, shielded head coil above ~100 MHz.

Tuning frequency shifts from *symmetric* loads (especially in whole-body and high-field *in vivo* animal research) often exceed the practical tuning range of a 2-point-drive birdcage by a factor of 3-15. Our experience agrees with published discussions that the maximum useful tuning range for a low-field 16-capacitor 2-point-drive birdcage is 1.3% and that it is inverse with the number of distinct capacitors, not rungs. The sample-induced tuning shift for a high-field whole-body coil can exceed 8% – at least 14 times the tuning range of a 12-rung hybrid birdcage, for example.

3.42 Theoretical Basis for the Software Model. None of the rf circuit simulation software that we evaluated several years ago directly handled multiple couplings in multi-line transmission lines (TRLs), nor did it easily handle the couplings and losses in transformers of more than two windings. Improved capabilities are now available in several high-end package (e.g., Genesys 8 from Eagleware) that better address these situations, but there are still serious limitations. So we chose to figure out how to effectively use a common, low-cost tool during Phase I. We plan to select more advanced circuit modeling software during Phase II.

In our model, all of the major parasitics are included and their effects are simulated for several 2-point and 4-point drive schemes for various loadings, detunings, and random errors. We should point out that our previous method [*2*] of representing all sample losses as stray capacitors C_S in series with resistors R_S leads to problems if $R_S > 1/\omega C_S$ and if the rungs are represented by inductors with coupling coefficients rather than transmission lines with coupling coefficients. This does not adequately respect the physics, and one of the manifestations is that the early model appeared more sensitive to rung errors than it should have.

Figure 7 illustrates the simplest circuit model (compatible with almost all rf circuit simulation software) that seems to give the accuracy needed for the 8 or 16 rung BHP birdcage or litzcage. To represent the nearest-rung couplings (L_C), each rung includes two ideal transformers, one on either side of the central plane – e.g., rung 2 includes {2,12,3,13} and {13,23,14,24}]. A transmission line (TRL) at each end of each rung completes its self-inductance and furnishes most of the significant stray capacitance per rung (e.g., {11,12} and {14,15} in rung 2).

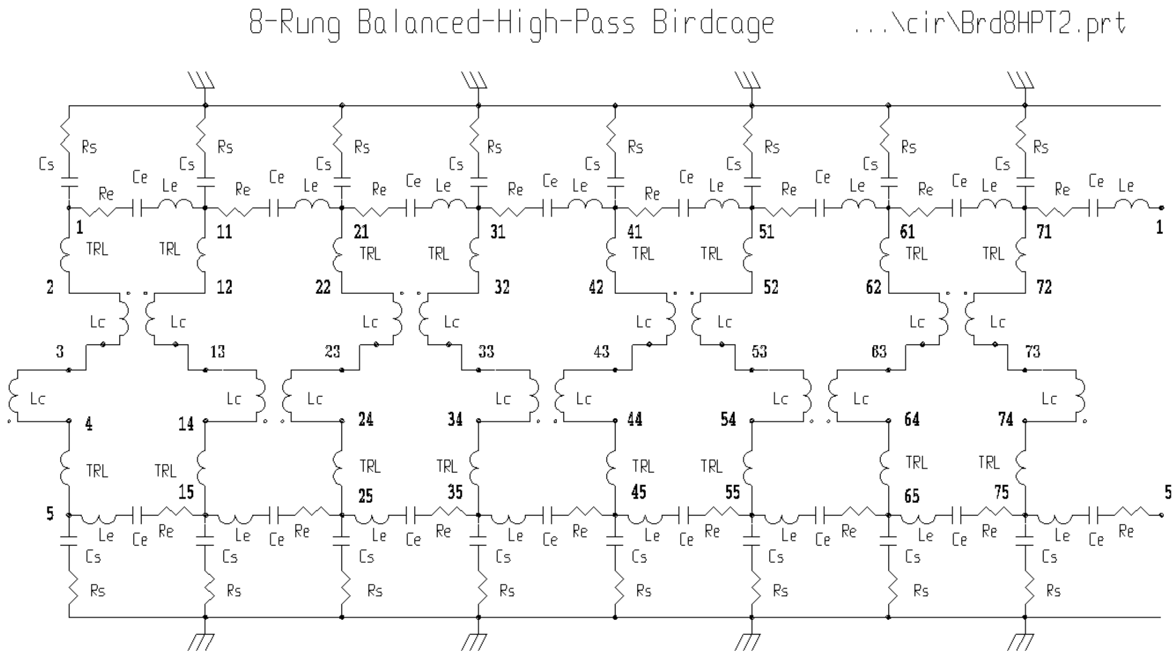

Figure 7. Our 8-section HP birdcage/litzcage model – less tune, match, isolation, and balance networks (see Fig. 9).

Before working on the full-size coils appropriate for human head and whole body MRI, it is useful to develop the rf circuit models from experiments on smaller coils that are more easily fabricated. We began with a 10 cm coil with a long, solid cylindrical shield of 14 cm diameter.

The division between the TRL and the coupling transformers representing the rung is determined as follows: First, the impedance of the TRL comprising the external rf shield and a single rung is calculated using a microstrip transmission line numerical model, such as that developed by Rogers Corp. (http://www.rogers-corp.com /mwu/mwi_java/Mwij_vp.html). For example, our 8-rung litzcage of 10.05 cm diameter has total rung width w (outside dimension of the two rungs per section) of 2.5 cm. When inside a shield diameter of 14 cm, the rung TRL impedance Z_0 is found to be 106 Ω for a propagation factor v of 0.9 (the dielectric constant of the polycarbonate coilform is 2.9, but the electric and magnetic fields for the lightly loaded coil are mostly in air).

Next, the inductance per unit length L_l (H/m) and capacitance per unit length C_l (F/m) are calculated according to the standard equations:

$$L_l = \frac{Z_0}{vc} \quad ; \quad C_l = \frac{1}{vcZ_0} \qquad (2, 3)$$

where vc is the propagation velocity. For the above example, L_l = 3.8 nH/cm and C_l = 0.35 pF/cm, or L_{TRL} = 32 nH and C_{TRL} = 3.0 pF for our rung length of 8.5 cm.

For comparison, the self-inductance L_0 for the isolated unshielded rung may be estimated [Grover, 1962],

$$L_0 = \frac{\mu_0 l}{2\pi}\left[\ln\frac{2l}{w} + \frac{1}{2}\right], \qquad (4)$$

and is found to be ~41 nH in this example. But the inductance of the rung as a microstrip TRL (32 nH) from eq. (2) plus the inductance of the litz cross-over (~4 nH) is a much more accurate estimate of the actual shielded rung self inductance. The mutual inductance of two isolated conductors of length l and center-to-center separation distance d may also be calculated [Grover, 1962],

$$M_0 = \frac{\mu_0 l}{2\pi}\left[\ln\left(\frac{l}{d} + \sqrt{1+\frac{l^2}{d^2}}\right) - \sqrt{1+\frac{d^2}{l^2}} + \frac{d}{l}\right], \qquad (5)$$

which amounts to 23 nH for the example dimensions. However, the presence of the external rf shield reduces the mutual inductance even more than it reduces the self inductance, and suitable published expressions cannot be found.

Yet, it is important to have an accurate estimate of the mutual inductance of the shielded rungs. This can be determined numerically using our *COILS* software. Several rungs, both single element and litz pairs, were numerically simulated to assist in estimating the mutual inductance between shielded rungs, for both full cylindrical shields and slotted shields, where the slot width in the shield is comparable to the space between the rungs and aligned therewith.

The total effective series inductance L_T was calculated numerically for two adjacent shielded rungs plus the connecting end-ring segments. The effective inductance of each connecting end-ring segment L_E was determined by assuming it to be constant as rung length changed, and data for long and short rungs was fitted to a linear equation. The mutual inductance M_{12} between adjacent rungs was determined from the basic relationship

$$M_{12} = (L_T - 2(L_{TRL} + L_E))/2 \qquad (6)$$

The simulation uncertainties are as follows: in L_T, ~3%; in L_E, ~5%; in Z_0, ~3% (for the solid rung with full shield).

Considerably more effort is planned for Phase II in numerically calculating mutual inductances for various geometric proportions (especially, relative rung widths and shield spacings) to allow us to develop more accurate empirical expressions for the end-ring inductance and rung mutual inductance. At this point, a useful estimate of mutual inductance M_S between adjacent, shielded rungs appears to be $(L_{TRL}/L_0)^3 M_0$, or 11 nH in this example.

Recall that for two coupled inductors of self inductances L_1 and L_2 and coupling coefficient k,

$$M = k\sqrt{L_1 L_2}\,. \qquad (7)$$

So if we represent the mutual inductance using transformers with k~1, they each add a comparable self inductance (11 nH, here) to the rungs. But only 4 nH needs to be added to each rung from the litz section cross-over, which is less than that added by the coupling transformers, so the inductance of the TRLs must be reduced. This can be done by reducing their length and their characteristic impedance appropriately. Expressed more precisely,

$$L_{TRL2} = (L_{TRL} + L_{CR})/2 - L_C\,, \qquad (8)$$

where L_{TRL2} is the inductance needed for each half-TRL in the model, L_{CR} is the inductance of the litz cross-over, and L_C is the mutual inductance to an adjacent rung. So L_{TRL2} is expected to be 7 nH, or ~40% of that calculated for the actual half-length TRL for the case of s=1.4 (recall s is shield/coil dia. ratio). Using TRLs in the model of lower impedance than originally calculated and shorter half-length gives the total self inductance needed with the coupling transformers added.

To re-cap, this adjustment in the TRLs is necessary because the rf circuit simulation software that we are using does not simulate coupled 4-wire transmission lines (i.e., a rung with 2 adjacent rungs and shield) directly. As s decreases, the mutual coupling decreases quite rapidly, so the 2-wire TRLs used in the model approach the physical dimensions of the rungs, but there are still limitations. In fact, it seems that we must go beyond nearest-neighbor rung couplings for a more accurate model. We are just beginning to refine our models with these couplings, which were not included in Figure 7 and most of our simulations.

3.5 The 3-ring 4-point-drive Birdcage/Litzcage

Our 3-ring high-pass (HP) coil geometry is illustrated in **Figure 8** (next page). The third ring is simply a copper foil ground ring on the coilform just beyond one end ring, to which all tune and balance capacitors and rf-line shields can be connected with minimal uncertainty in ground potentials and parasitics, making it much easier to control symmetry and uncertainties associated with the tune, match, isolation, and balance adjustments.

In many cases (for example, in the coil of immediate interest, the head coil), it is necessary to permit maximum access from one end of the coil to the sample region. Hence, the ground ring must be omitted at one end, which we will denote the **access end**. The other end will be denoted the **tuning end**. (Alternative terminology may be proximal and distal respectively.) For coils larger than ~6 cm diameter, it is generally necessary to capacitively segment the ground ring, but that can always be done in such a way as to have negligible effect on tuning behavior.

The gap between the ground ring and the tuning ring is typically ~10% of the coil diameter, and each node at the tune ring is connected to the ground ring via paths of approximately equal impedance. For the 8-section litzcage for example, we number these nodes 1, 11, 21, 31, 41, 51, 61, 71, as shown in Figures 7-9. The presence of the third ring moves the center of the field region slightly away from the geometric center between the access and tuning rings (toward the tuning ring), but the B_1 homogeneity in transverse planes is not affected as long as reactances in each of the 8 paths from the tuning ring to the ground ring are nearly equal.

We used the novel 4-point feed circuit shown in **Figure 9** (next page) in most cases. Here, the impedances to ground are controlled at 6 nodes {1, 11, 21, 31, 41, 61} rather than the customary 2 nodes {1 and 21}. While the first impression may be that this 4-point-drive circuit increases difficulty and unpredictability, it will soon become clear that the opposite is true on both accounts. (We note that this circuit is equally advantageous for conventional 8-section and 16-section HP and band-pass birdcages, but it is **not** compatible with 12-section birdcages (or litzcages) because of the importance of impedance control at 45^0 with respect to the feed planes. Interestingly, our simulations show 12-section birdcages are actually more difficult to tune and symmetrize than 16 section birdcages incorporating our 6-

point-control network.) An alternative 4-point-drive circuit was also evaluated briefly and shown to have advantages in cases where (1) the radial space between the coil and the shield is too small to easily accommodate the required variable capacitors and coils or (2) the coil diameter is much less than λ/4.

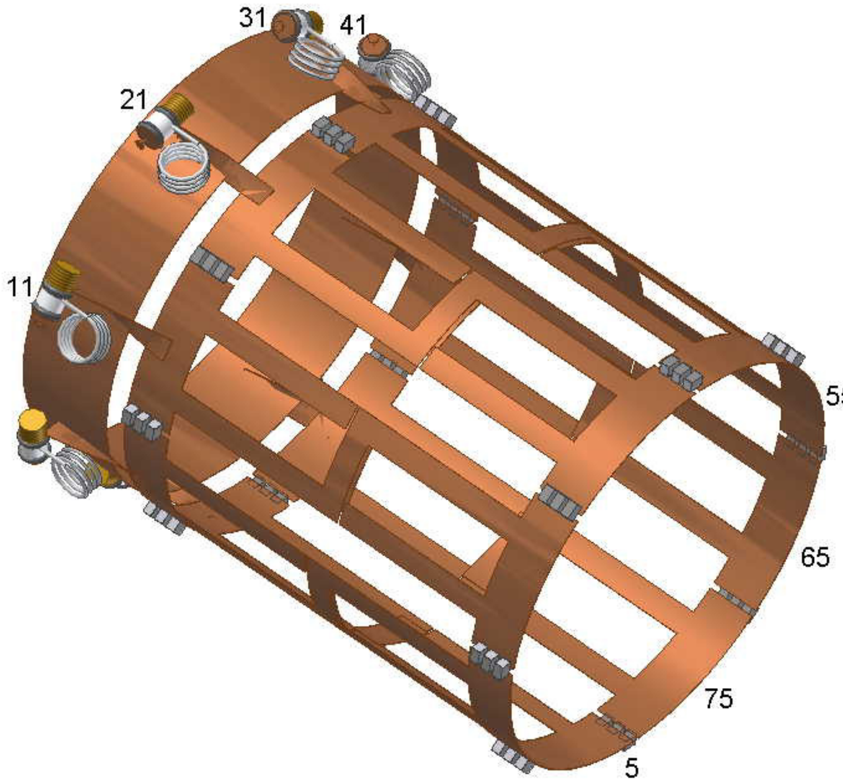

Figure 8. The 8-section high-pass Litzcage with a third (ground) ring configured for tuned 4-point drive. (The eddy-current-blocking capacitors in the 3rd ring and much of the balancing network are not shown.)

We have evaluated a number of birdcage variations (including the standard topology with the standard coupling methods – inductive, capacitive, and balanced capacitive) by comparing the predicted and measured frequencies of the principle modes. We eventually concluded that the addition of a ground ring (at the coil diameter) at one end, a short distance beyond the coil-structure ring, offered substantial advantages in the control of symmetry and parasitics compared to alternative ground references (e.g., an annular ring at one or both ends, remote references, the external cylindrical shield, etc.) for the tune, match, isolation, and balance adjustments. We now use this grounding approach exclusively in all of our low-pass, high-pass, and band-pass circular-polarization coils. Several straps (usually 8) of low inductance (~3 nH for the 10 cm experimental coils) connect this third ring to the external rf shield at the tuning end, but that still does not make the external rf shield a very suitable ground reference for the tuning and isolation controls, partially owing to the more complex potential map that is induced on this surface but primarily because of manufacturing reasons.

The tune/match/feed connections are made at nodes 1 and 41 for channel A and nodes 21 and 61 for channel B. Isolation adjustments connect at nodes 11 and 31. Extended tune/balance adjustments connect at nodes 41 and 61, and fixed balance capacitors connect at nodes 51 and 71. Capacitors C_{EC} serve only to block gradient eddy currents and have negligibly small rf impedance. The lead inductances L_L are quite small, so to a first approximation, each pair of series quarter-lambda's forms a center-tapped half-lambda between two nodes 180^0 apart on the tune

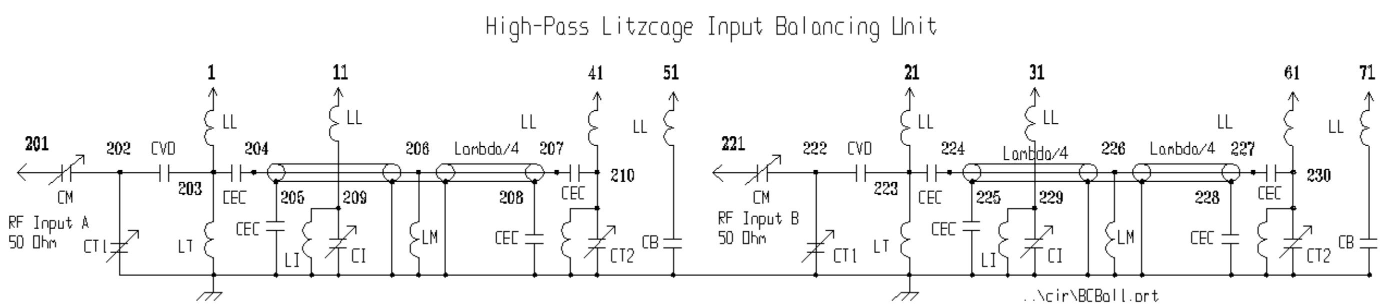

Figure 9. Complete schematic of the original 4-point-drive balancing network used above.

ring. The center-taps (where the impedance is very low at the homogeneous mode m_1) permit the attachment of a small inductor L_M for the suppression of a common (inhomogeneous) mode that otherwise appears (both in the models and in the experiments) near m_1. Ideally, the impedance appearing at one end of a half-lambda is reflected to the other end, so the second set of tune variable capacitors C_{T2} would seem to be redundant with the first pair, C_{T1}. However, the ground is not ideal, so improved symmetry (isolation and homogeneity) is observed from dividing this tuning adjustment. But C_{T1} and its respective C_{T2} need not be very close to the same value. They are essentially parallel tune adjustments. Variable capacitors for optimizing channel isolation are needed only at one point on the plane mid-way between the two feed planes and at one point on the orthogonal plane. Hence, tune, match, and symmetrization (isolation, homogeneity, and balance) may be unambiguously optimized with 3 largely orthogonal (weakly interacting) adjustments per channel.

For high homogeneity and channel isolation, the peak variation in impedance δZ_i to ground among all nodes at each end must be very small compared to the impedance of the section ring capacitor, $(\omega C_i)^{-1}$. The allowable relative errors (which, for high-field coils will come more from sample asymmetries than from manufacturing tolerances) depend strongly on the number of sections and the type of control network implemented. We limit our remarks initially to 8-section balanced high-pass coils, and these remarks apply equally to birdcages and litzcages.

The sign of a single impedance variation at any node is immaterial in the magnitude of the inhomogeneity it produces, so a factor of two increase in adjustment range is readily obtained by tuning out half the capacitance of the variable capacitors utilized in the tune, match, balance and isolation variables for an effective adjustment range of -4 pF to +5 pF ("zero-center" variables). However, it is critical that the coils utilized for this purpose (e.g., L_T, L_I in Fig. 3) not couple strongly to the fringe field of the litzcage, or other modes arise. If these small tuning coils are oriented with their axes radial and positioned mid-way between the ground ring and the external rf shield, they will be orthogonal to the fringe fields from the litzcage during both linear tune-up and CP operation. Otherwise, they must be shielded.

The importance of properly including the effects of the ground ring and external shield on the effective inductances and stray capacitances of the tune-coils at the six control nodes can hardly be overstated. The stray capacitance is easily determined with sufficient accuracy, so the desired effective inductance with the variable capacitors at mid-range can then be calculated. The resonant frequency of each separate node control circuit (e.g., LI, CI) at mid-range with LL disconnected can then be calculated. The only way to achieve adequate balance is to verify these individual frequencies with the external shield in place.

As shown in Fig. 7, each ring section is represented by an RLC circuit (LE+CE+RE). The lossy stray capacitance from each end node to the sample (CS+RS) is also shown. The stray capacitance from the center of each rung to the sample (e.g., {13, 0}) is also included in the model though not shown in the schematic (to reduce the clutter). Each rung is represented by two coupling transformers to adjacent rungs and a transmission line of appropriate length at each end.

3.51 HP Litzcage Experiments. A large number of experiments were performed on various 8-section HP litzcages of 10 cm diameter with 8.5 cm (inside) rung length for a variety of frequency, load, shielding, and coupling conditions. Data were tabulated for three different feed schemes: severely undercoupled, 2-point unbalanced capacitively coupled, and the balanced 4-point method of Fig. 9. The shield/coil diameter ratios *s* were either 1.2 or 1.4, and both full cylindrical and windowed shields were tested at frequencies from 200 MHz to 470 MHz. Experiments with 17-cm band-pass (hybrid) litzcages were also performed at 170 MHz and 270 MHz to begin development of a circuit model appropriate for whole-body coils at 3 T. We then proceeded to the 28 cm open-access head coil at frequencies up to 180 MHz. In all cases, the capacitors were measured and matched within $\pm$1.5% or $\pm$0.15 pF, whichever was greater; and the shield-to-coil radial spacing and rung dimensions were controlled within ~1%.

Some of the loaded experiments were done by placing equal-value fixed resistors across each CE at one end so that the sample region was available for field mapping, and some used a 30 mM saline load of 75 mm diameter and 85 mm length. The undercoupled (UC) data were obtained using a small pickup loop with no tune/match network connected to the coil. The maximum tuning range Δf_{max} in MHz using the tuning variables and the frequency shift df_0 caused by the sample were also measured, as were the loaded and unloaded Q's and magnetic filling factors, from which the power requirements for a 1 ms pw90 were calculated by the method previously described [*2*].

Channel isolation ψ_0 was measured at the center of the tuning range after adjusting the two isolation variables. Then, the two channels were tuned to the top end of the adjustment range using only the 2 or 4 tune variables and matched to 50 ohms using the 2 match variables for the isolation data here. The channel isolation ψ_2 was measured without readjustment of the isolation controls from their optimum midrange settings. The two isolation variables were then adjusted for maximum isolation ψ_{2A}, and the corrected isolation ψ_{2A} noted. The two channels were then tuned to the low end of the adjustment range and the above measurements repeated. The mean isolation at the limits of the tuning range both prior to (ψ_2) and after (ψ_{2A}) adjusting the isolation variable capacitors were recorded. The peak B_1 inhomogeneity (σ_0) was also measured (to the best of our ability) at the center frequency, at the lower frequency limit (σ_1), and upper frequency limit (σ_2) with the isolation variables at their initial (central) value. This was compared to the calculated relative peak rung current variation *di*, where $di=(i_{max} - i_{min})/i_{mean}$) at the tuning limits.

We measured B_1 homogeneity on the bench using a variety of published and proprietary methods but with insufficient accuracy for meaningful comparisons to the model calculations. Very recently, we completed the fixturing and instrumentation necessary to implement a novel bench method of rf field mapping which appears to be much more accurate and reliable than prior methods. A small, conducting disc is rapidly rotated about an axis perpendicular to B_1 (parallel to the coil axis) inside the slightly mismatched coil at the location being probed. The S11 test signal (at f_0) is detected (demodulated) and then amplified through an audio preamp followed by a band-pass filter. The amplitude of the detected audio signal is proportional to a number of factors, one of which is the local magnetic filling factor –

hence, field strength. The coil is mounted on an X/Y/Theta control table and the rotating disc position is controllable in the Z direction (i.e., a modified drill press) to facilitate field mapping throughout the coil. The method works only for a linearly polarized field, so the two channels must be tested separately. Continued efforts focus on addressing the complex nature of this bench measurement, including the confounding effects of radiation, mean mismatch, and local E fields. However, the technique appears to be usually better than alternative methods and will be published in the near future. A small subset of some of the experimental data at 400 MHz appears in Table 1. Interestingly, considerably better homogeneity was measured in this coil when tuned to ~470 MHz with *s*=1.2 and a windowed shield.

Table 1. High-pass 3-ring 8-section Litzcages, *s*=1.4: **Experimental Data**
10 cm dia. x 8.5 cm long coil, with full (long) cylindrical shield of 14 cm diameter

Exp. #	feed	*f*	Load	Q	Range Δf_{MAX}	Isol. ψ_0	Isol. ψ_2	Isol. ψ_{2A}	σ_0 %	σ_1 %	σ_2 %	m_{1+}	$\mathbf{m_1}$	m_{2+}	$\mathbf{m_2}$
		MHz			MHz	dB	dB	dB	-	-	-	MHz	MHz	MHz	MHz
1.11	UC	~400	-		-	-	-	-	-				410		
1.12	2-pt	~400	-	184		25	10.2	16	9	13	7	-	404.2	367	343
1.13	4-pt	~400	-	168	22	35	18	24	8	10	10	430	402.5	344	324
1.14	4-pt	~400	390Ω	20.4	24.7	40	26	33	5	14	8	425	398.4	342	322
1.15	4-pt	~400	saline	9	23	48	30	45	-			425	384.8	344	320

Initial estimates for circuit variables LC, LE, and CS and the TRL characteristics (Z, *v*, α, lgh) were obtained by the methods discussed earlier in section 3.32. These values were then adjusted to improve the fit of the calculated circuit response (m_1, m_{1+}, m_{1-}, m_2, m_0, Q_0, Q_L, *di*, Δf_{max}, df_0, C_M) at the frequencies to which the coil was tuned (e.g., 200 to 470 MHz).

3.52 Conclusions from Experiments and Simulations on Small HP Litzcages. Because of space limitations imposed on this Phase I Final Report (and partially because of uncertainty in the B_1 homogeneity data), we do not include much of the raw data, but instead discuss the general characteristics and unambiguous conclusions. First of all, the homogeneous mode m_1 was generally predicted within ~1.5% over the full range, and the nearest inhomogeneous mode (for the 4-point-drive circuit on the HP litzcage this was m_{1+}, usually ~15% above m_1) was generally predicted within 3%. Isolation at the center of the tuning range (both channels tuned to the same frequency within f_0/(10*Q)), with minor adjustments (usually, <1.5 pF) on CI, was typically ~25 dB for 2-point drive at the higher *fd* products and ~35 dB for *fd* below ~25 MHz-m. Isolation generally improved ~5 dB for 4-point drive.

The model and the experiments show that the 16-rung birdcage's sensitivity to small asymmetries lying 22.5^0 from one of the feed planes agree adequately with the first-order theory. However, the effects of perturbations along a feed plane or 45^0 with respect to a feed plane are much more severe than predicted by the first-order theory with respect to B_1 homogeneity and channel isolation respectively, especially for 2-point drive.

The primary disparity between the experimental and the simulation data is in the simulated isolation when rung errors are supposed to be zero. The reason is simply that experimentally, the rung errors (L or C) are not easily kept below 1.2%, and this is barely sufficient to achieve 20 dB isolation without correcting the isolation variables, CI. In fact, the deviation of these variables from their optimum value must be less than ~0.2% of C_E for isolation to exceed 40 dB for an otherwise perfect coil. While 40 dB isolation in itself is not needed, there is a very valid indirect reason to try to achieve this: The best simple indication of B_1 homogeneity appears to be the maximum isolation that can be achieved with careful adjustment of the CI variables. To explore this relationship, we simulated a number of error combinations on various coils and we report our conclusions here.

Suppose the mean effective total section capacitance at one end is C_{ET} and this total is precisely present at each node except one, which has total capacitance C_{ER}. (Note that by total section capacitance, we mean the value of C_E for the conventional simple model in the absence of stray and TRL capacitance.) We define d_{CR} as the relative capacitance error (deviation from mean section value) at one end as d_{CR} = ABS((C_{ET} - C_{ER})/C_{ET}).

We can draw some general conclusions about the relationship between relative capacitance errors and relative peak-to-peak current errors *di* (as before, $di=(i_{max} - i_{min})/i_{mean}$) for various situations. In all cases, both channels are tuned to the same frequency within f_0/(Q*10) MHz, or ~0.03% for the Hi-Q examples and ~0.2% for the low-Q examples. For the balanced 8-section HP coil with 2-point drive, a single capacitor error of 4% (of C_{ET}) introduces a typical splitting of ~0.25%. For balanced 4-point drive, the splitting is typically ~0.15%. So the single-rung capacitor errors are restricted to very small values in the Hi-Q cases. Some results are:

A. For 2-point drive (no λ/4 lines), Q=350, *single rung error*: For isolation = 20 dB, *di* is 3 to 5 * d_{CR}, depending on location of error. For isolation = 30 dB: *di* ~ d_{CR}. For isolation = 40 dB, *di* ~ d_{CR}/2.
B. For 2-point drive, Q=350, *two rung errors, **un-lucky** combination*: For isolation = 20 dB, *di* ~ *5* * d_{CR}.
C. For 2-point drive, Q=50, *single rung error*: For isolation = 40 dB, *di* ~ d_{CR} + k_i, where k_i is 0.05 to 0.1

For larger capacitor errors, one observes greater current errors at higher isolation than indicated by the above. Note that in all cases we have adjusted the isolation variables for best possible isolation. While the most obvious effect of this adjustment is that it typically (for the loaded coil with 2% capacitor tolerances) improves isolation from ~14 dB to ~30 dB, it also (according to the model) typically reduces rung current errors from ~15% to ~3%.

With our 4-point drive (center-tapped $\lambda/2$ network), all of the above relative-rung-current errors are reduced by nearly a factor of 2 on average, and worst-case errors are reduced by up to a factor of ~4. Minimizing rung current errors is critical in maximizing SNR, as near field SAR is quadratic in rung current errors.

For fifteen years, it has been accepted that symmetry in principle could be improved by using 4-point drive [*30, 31*], but technical difficulties have usually prevented it from being implemented. One problem is that it inevitably introduces at least one additional inhomogeneous mode, and it is often too near the homogeneous mode. In fact, it may be close enough to make matters worse. With the circuit of Fig. 9, the parasitic mode is easily moved far enough away (usually 10-15% above) with a small value of L_M. The characteristics of the phasing lines are not critical. Obviously, low loss lines are preferred, especially for low-load conditions, where phasing-line losses might exceed 25% if care is not exercised; but for high-load conditions, the losses added by the phasing lines are easily kept below 1-2%. Much more important than the attenuation constant, impedance, and velocity factor are the routing and grounding conditions. Eddy-current-blocking capacitors are generally required, and it is critical that the cables and ground connections at the cable ends not have significant coupling to the fringe field of the tune ring.

The maximum tuning range with our 4-point drive network with acceptable B_1 homogeneity, is about ~3.5 times that obtained with two-port drive for an 8-rung birdcage *with* zero-center (tuned) variable capacitors. It is ~5 times that obtained on a 12-rung birdcage with zero-center tuning and accurately balanced nodes, and ~15 times that obtained by the standard (2-point) tune/match capacitor-only circuit on a 16-rung balanced HP birdcage.

3.6 The Axially Asymmetric Semi-Open Tunable Litzcage Head Coil

The head coil optimization is somewhat unique, owing to the presence of the neck and shoulders at one end and free space at the other end – which has been called the "top end" or the "distal end". We will now begin calling it the "tune end", for reasons that are apparent from Figures 8 and 10. The other end, which has been called the "shoulder" or "proximal" end, we denote the "access end".

While an rf mirror at the tune-end of the head helps S/N a little by reducing radiation, it also severely restricts access to the head. There is no doubt that a mirror at the top of the head improves B_1 homogeneity and S/N substantially in this region for a *short* coil. However, our simulations indicate the same improvement in both is possible by simply extending the coil well beyond the head *if* radiation is suppressed by lengthening the external rf shield. Indeed, lengthening the coil makes it a little more difficult to tune at very high fields, but there seems to be no other way to obtain the needed openness without sacrificing performance. Increasing the ring width at this end also helps (both with S/N and with the upper practical *fd* limit), and the addition of the wide ground ring on the coilform diameter (see Fig. 8) helps reduce radiation.

Figure 10 (next page) illustrates the completed semi-open broadly tunable head coil, viewed from the tune end, as developed and bench-tested during the Phase I. (The patient's body would extend from the remote end in this view, which is opposite the view of Figure 8. The tuning rods may be short or long, depending on the user's preference.) The eight long wide slots between alternate rungs of the litzcage and the absence of the rf mirror provide a degree of openness and sample access not previously available in high-performance MRI coils. The effectiveness of the shielding is such that the shift in f_0 (at 128 MHz) is less than 0.3% when the head coil is moved into a 43 cm diameter cylindrical copper shield, simulating a large head gradient coil.

The balanced 4-point-drive HP litzcage shown in Figures 6-9 was used, and the coil was bench tested at 66 MHz, 125 MHz, and 180 MHz under various load conditions. The windowed rf shield is etched onto ½ oz copper-clad double-sided kapton. With an axially asymmetric shield, to prevent excessive B_0 gradient eddies during EPI, 8 eddy-current-blocking slits along 8 lines bisecting the 8 windows are used, and the required rf capacitors are formed directly into the substrate.

While the operational robustness (tune/load range, isolation, and ease of tune-up/symmetrization throughout the load range) of some commercial 3 T head coils meets many requirements, it appears that our coil exceeds the best prior technology in this regard by at least a factor of two; and it probably exceeds most commercially available coils in robustness by a factor of 4 to 6. The openness of our coil also exceeds that of prior 3 T coils by a similar factor.

Our business record of being able to sell ^{1}H/X MRI small-animal coils at 30% to 50% less than the price of our competitors, along with our experience during the Phase I in the development of this head coil, lends credence to our expectation of being able to sell this head coil substantially below the price of current state-of-the-art commercial head coils for 2 to 4.7 T. For example, the demo head coil was tuned to 130 MHz, then to 66 MHz, then 180 MHz, and then tuned back to 125 MHz, all in the space of ~15 days, primarily by one technician on this project. In all cases 4-point drive was implemented. At the same time, extensive bench tests were performed at all frequencies. (See Product Development section for a photo.)

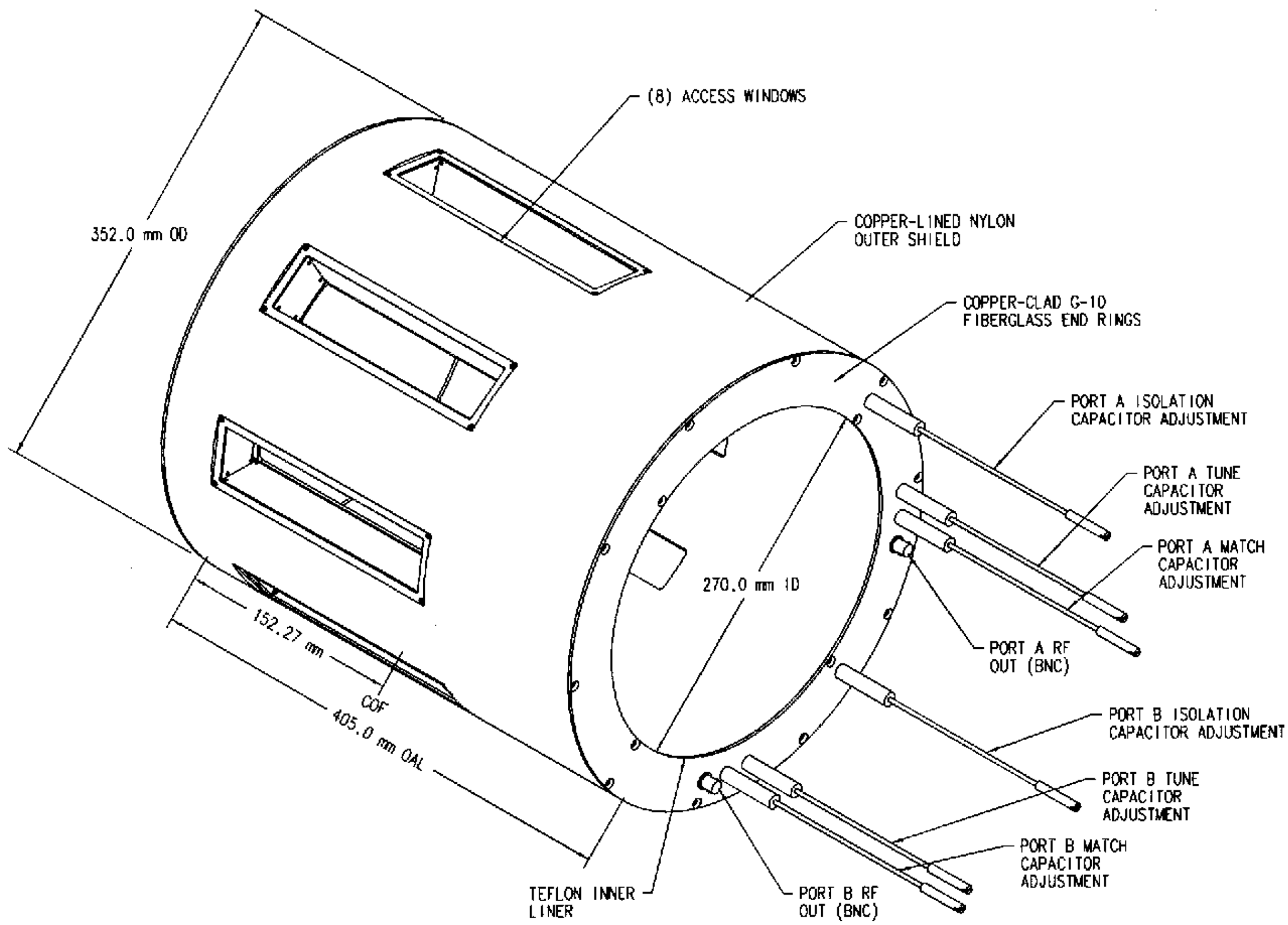

Figure 10. Perspective view of the semi-open prototype tunable head coil, as constructed and tested.

Table 1 summarizes some of the test results for 4-point drive (except Q_0, which was measured with 2-point drive). The isolation listed is the worst-case (minimum dB magnitude) measured over the full tune range and load range for 4-point drive. The nearest parasitic mode m_{1+} is also listed (m_0 is quite a bit higher). Q_{L1} was measured with a 2-liter Coke bottle filled with normal saline (150 mM) on center, and Q_{L2} was measured with a centered 1-gallon plastic milk jug filled with 100 mM saline. These loads approximate the load range from a light patient to a very heavy patient. The power required to generate a pw90 of 500 µs using a square pulse was calculated from the *measured* Q_{L1} and *measured* η_F, according to previously published methods [*2*]. (The simulations gave considerably higher η_F. These discrepancies have yet to be resolved.)

We have only been able to locate sufficiently detailed published data to permit unambiguous SNR comparisons from bench measurements *without proprietary test probes* for one modern head coil – the Siemens 1.5 T coil [*38*]. **These results indicate our SNR improvement compared to the Siemens coil for median load (3 L normal saline) is at least 4.5 dB at 1.5 T. The data also show that Q-ratios alone are inadequate measures of coil performance.**

f_0 or m_1 MHz	m_{1+} MHz	C_E pF	$C_{TuneVar}$ pF	TuneRange MHz	LoadRange Q_0/Q_{MIN}	Isolation dB, min.	η_F, %, V_S=2 liter	Q_0	Q_{L1} 2 L	Q_{L2} 3.8L	P_1, W, τ_{90}=500µs
66	92	88	2-25	0.6	5	23	0.55	660	165	98	40
125	145	23	2-20	4.8	15	17	0.52	470	106	53	160
180	203	8.3	1-10	2.5	4	16	0.5	280	88	52.5	290

3.7 The Band-pass (BP) Litzcage for 2-4 T Body and 5-8 T Head Coils. The upper practical frequency for the high-pass litzcage head coil (Fig. 6) is ~200 MHz, but the concept is readily extended to higher frequencies by utilizing the so-called hybrid or band-pass filter method as shown in **Figure 11**.

This approach seems preferable to increasing the number of high-pass litzcage sections from 8 to 16, as the 16-section high-pass requires more capacitors, has a smaller tuning range, has a lower practical frequency limit, and has higher axial electric fields within the sample. The disadvantage of the hybrid is that it is much more difficult to

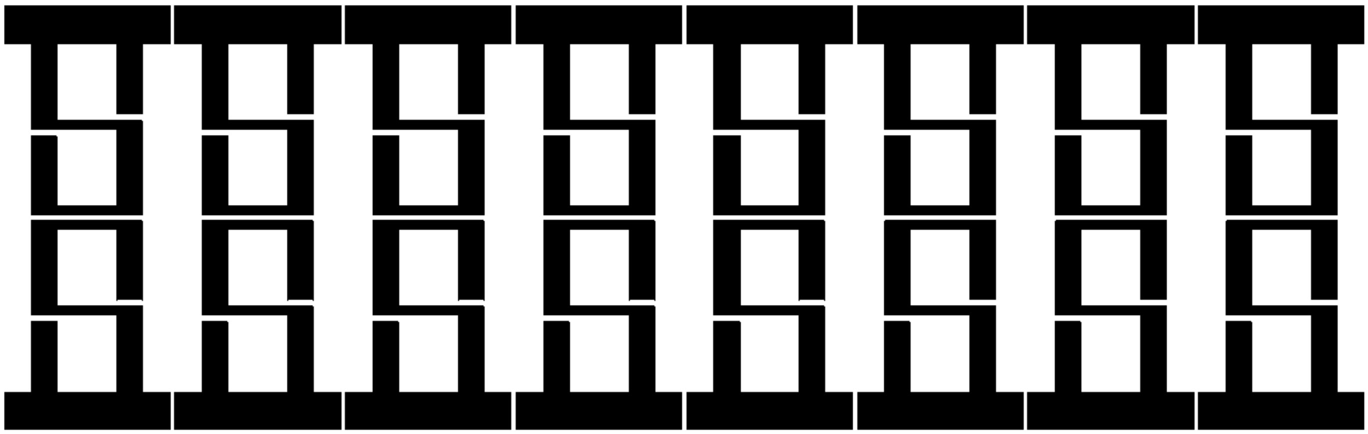

Figure 11. The primary pattern of the band-pass litzcage. The upper and lower crossovers are completed on a second surface. Capacitors are inserted into the central and ring gaps.

avoid parasitic modes near the homogeneous modes. We expect the hybrid litzcage to be selected for *fd* greater than 40-60 MHz-m, depending on the relative coil length and *s*. Above ~60 MHz-m, the four $\lambda/4$ lines used in our original 4-point-drive network (Fig. 9) must be replaced with four $3\lambda/4$ lines (which complicates stray field interactions) or an alternative circuit must be used. We have looked at a number of alternative 4-point-drive balancing circuits and have begun evaluating one promising option which uses four $n\lambda/2$ lines from the litzcage to a remote balancing network, which is based on two $\lambda/2$ lines. This second network has been satisfactorily tested with a 470 MHz 26 mm low-pass litzcage, and tests are beginning on large HP and hybrid litzcages.

To test our model predictions that the 4-point-drive hybrid litzcage will enable substantial advances in performance and robustness of large MRI coils at the highest fields, we constructed a 17.5 cm diameter band-pass litzcage with a full cylindrical shield at *s*=1.2. The inner rung length was ~14 cm. The coil was first tuned to 170 MHz, and then 270 MHz. (A body coil would normally have relative length ~30% less and *s*~1.12, so this 17.5 cm litzcage at ~300 MHz would be a reasonable scaled model of a 3 T body coil.) The model predicted the frequency of the homogeneous modes with reasonable accuracy (~5%), but there were large discrepancies in the predictions of the nearby inhomogeneous modes and isolation. This makes it very difficult to have any confidence in the B_1 homogeneity predictions of this hybrid model.

From these preliminary experiments, it was clear that a more detailed circuit model than a simple extension of Figure 7 (inserting segmenting capacitors between the central coupling transformers) needs to be developed for the hybrid litzcage. We obtained a demo license of Genyses 8 (widely reputed to be the most advanced rf circuit software) from Eagleware and began building a more detailed rf circuit model based on coupled microstrip lines. Some preliminary results were encouraging, but it also became clear that there are serious limitations with this software and considerable effort will be required during Phase II before we will have a satisfactory circuit model for the hybrid litzcage. We plan to evaluate several other circuit software options during Phase II before making a selection and proceeding with this critical model development for the 50-100 MHz-m range.

3.8 Other Phase I Work. In addition to the above reported tasks and developments, other work carried out under this Phase I involved rf magnetic field calculations on litz coils, birdcages, and litzcages. Simulations were also carried out on passive and active high-order B_0 shimming on the human head. Finally, experiments on 4-point-drive low-pass litzcages that demonstrated advantages for small-animal imaging were carried out at 200-470 MHz. Much of this work forms the basis of the following Phase II proposal.

4.0 Phase II Proposal: High-Throughput RF Coils for High-Field MRI

The initial Phase II priority will be field testing and productizing the above 3 T head coil, but further model development is also needed to facilitate other more challenging coils, especially for knee and torso. The progress reported above would not have been possible without our ability to rapidly and accurately simulate complex circuits and complex coils. Birdcage models have been simulated by various groups showing effects of sample conductivity and permittivity [*9, 20, 32*], but the simulations have included major assumptions: no input/output matching circuits, idealized tuning, lossless conductors and capacitors, and usually a relatively small sample. Our simulations (which drop assumptions of lossless circuits, and idealized tuning and coupling but retain long-wavelength assumptions and simplified loss models) have been the first to include calculation of magnetic filling factor η_F, unloaded Q_0, and loaded Q_L and thus the first (and perhaps still the only) to permit reasonably valid estimates of S/N as well as B_1 homogeneity [*2*].

We feel that the most significant shortcoming of the prior FEA and FDTD simulations we are aware of (those reported in *MRM*, *JMRI*, and *JMR*) is that they apparently exclude most or all of the tuning and matching elements. Almost all have inserted idealized voltage sources between each conductor element to achieve the ideal phase relationships at these points. A recent simulation [*33*] (and perhaps others) takes an important step toward addressing this shortcoming in the standard methods [e.g., *20*, *32*] by feeding the coil from ideal voltage sources at only the four actual capacitor feed points around the coil, rather than the standard method of 1, 2, or 3 defined voltage sources per rung. Still, this ignores the circuit issues of obtaining the precisely balanced 180^0 drive signals without introducing another closely spaced mode. We previously reported excellent agreement between our measurements and simulations of Q_0, Q_L, η_F, rms B_1 inhomogeneity σ_B , and SNR for a number of balanced-high-pass (BHP) 10 cm birdcages at 200 MHz with an asymmetrically placed saline load (35 mMolar, or 0.3 S/m) [*2*]. A number on enhancements were made in the software during the Phase I, and we report some of these advances here.

4.1 *COILS* 6.1: Current Distributions in Complex Coils. As we have not publicly released our software, dubbed *COILS*, it is understandable that there could be some misunderstandings of its capabilities, so it seems appropriate to make a few comments here. Simple Biot-Savart-only software generally provides only a DC solution, but that is not an accurate description of our software. At DC, current distributes itself among parallel conductors such that the total power dissipation is minimized. However, when the inductive reactance is large compared to the DC resistance (as is the case in all high-Q coils) and when the conductor element length is less than lambda/2, current distributes itself among parallel conductors (or across the surface of an extended conductor) such that the total magnetic energy is minimized. We refer to the second condition as the radio-frequency condition, and it generally applies to MRI coils. Each of the above principles can be readily derived from circuit theory. Alternatively, the DC rule can be argued from the second law of thermodynamics. In the absence of dielectric and magnetic materials, the only long-wavelength boundary condition imposed by Maxwell's equations for the case where the conductor thickness is large compared to the rf skin depth is that the normal component of B_1 vanish at the surfaces of conductors. Our software is capable of adjusting (either automatically or manually) the current distributions such that these requirements are satisfied. The resulting rf current distribution typically differs from the DC solution by several orders of magnitude. One check on the validity of the calculations is the agreement between the measured and experimental inductance. Our simulations typically give an inductance that agrees with experiment within ~2%. Our simulated unloaded and loaded Q's (which of course cannot be calculated with a DC code) for arbitrary coils and samples typically agree with experiments within ~15% for the full range of sample sizes and frequencies normally encountered, both in volume and in surface coils.

The rung conductor length between segmenting capacitors in a whole-body hybrid birdcage at 3 T (as depicted in Figure 3) is likely to be ~16 cm (the axial length of uniform gradients in short high-field magnets is only 30-34 cm). The free-space wavelength at 128 MHz is 2.34 m, so the conductor element length is ~$0.068\lambda_0$. It is important to appreciate that it is the distance between segmenting capacitors, not the total circuit path length that must be less than $\lambda_0/2$. Most of the oscillatory energy exchange (up to the fraction (Q-1)/Q of the energy exchange) is between adjacent inductor and capacitor elements, and it is the Poynting vector velocity between these locations that is limited to *c*, not the circuit phase velocity [*34*]. Correcting for both losses and stray capacitance, a more practical limit on the individual conductor element lengths for circuit validity with our methods is ~$\lambda_0/3$.

Indeed, the wavelength in the tissue is less than in free space by a factor of 8-9, but rf magnetic filling factors are typically ~5%, and analogous "electric filling factors" are typically 6-20%, so the sample's effect on the coil circuit frequency is typically less than 10%. Of course, sample dielectric effects will be significant on the relative magnitudes of the fields calculated in the sample, and these effects are not well addressed by our software. Still the unloaded and loaded Q's we calculate for the short-wave-length conditions show better agreement with experiment than the examples we have seen thus far from full-Maxwell 3D commercial software (XFDTD, Remcom, Inc., State College, PA; and EMAS, Ansoft Corp.).

Perhaps even more striking than the accuracy and flexibility of our *COILS* software is its speed. For a surface coil for example, once the surface current distribution is determined (which may take a few hours), we calculate the **B** and **A** fields (and approximate **E** field) throughout space, unloaded and loaded Qs with a specified sample, and L, all in 15-30 seconds (without using any previously calculated field vectors). Some commercially available full-Maxwell 3D software (Finite Difference Time Domain, XFDTD, Remcom) typically requires 2-20 days (depending on the frequency and accuracy) for this calculation on a comparable platform. It's advantage is improved accuracy in the determination of the **B, A,** and **E** vectors within the sample region for the short-wavelength condition. Clearly, FDTD methods are useful in obtaining a more accurate evaluation of the performance of a given coil design, especially for a complex tissue sample when wavelengths within the sample are less than twice the transverse sample dimensions.

4.2 Losses in Complex MRI RF Coils. The computational difficulty of this problem may be appreciated by noting that the element size for a conventional FEA approach must be about a micron (a fraction of the classical skin depth) near critical surfaces in portions of the conductors, but the rf fields often extend over tens or hundreds of millimeters. Even for a small coil with a highly sophisticated meshing algorithm, the complete 3D FEA solution requires a minimum of several million elements. An augmented Biot-Savart approach, on the other hand, has the capability of quickly solving rf coil problems with arbitrarily oriented conductors. As noted earlier, the current distributions are not initially known and must be determined in an iterative fashion (energy minimization) that can be extremely time consuming with commercial software.

Our *COILS* approach is to describe all currents (whether actively driven, induced by changing fields, or induced in magnetic materials by static fields) by a collection of common geometries. These coils are each broken up into thousands of integration element vectors. Field vectors are calculated separately for each coil, and the vector field contributions from each coil to each point in space are stored along with the composite field in a way to permit rapid recalculations when a portion of the system is changed. From the Biot-Savart law, the field contribution $d\mathbf{B}(\mathbf{r}_f)$ for current element $I_i d\mathbf{l}_i$ at $\mathbf{r}_i$ is given by

$$d\mathbf{B}(\mathbf{r}_f) = \frac{\mu_0}{4\pi}\left(\frac{I_i d\mathbf{l}_i \times (\mathbf{r}_f - \mathbf{r}_i)}{|\mathbf{r}_f - \mathbf{r}_i|}\right) \tag{9}$$

Of course, the above is accurate only in the absence of dielectric and magnetic materials and for distances small compared to $\lambda/4$. But as we previously showed, while the fields calculated within the sample region may have significant errors (and subsequent corrections will be required), the effect on the coil tuning behavior remains minimal in practice because 90-98% of the oscillatory energy exchange per cycle in practical coils takes place over distances that are small compared to $\lambda/4$, even for whole-body coils at the highest available fields.

The induced potential throughout the sample is given by the sum of the conservative electric field ($\nabla\Phi$) and the time derivative of the vector $\boldsymbol{A}$ potential field, which is given in differential form at long wavelengths by the following:

$$d\mathbf{A}(\mathbf{r}_f) = \frac{\mu_0}{4\pi}\left(\frac{I_i d\mathbf{l}_i}{|\mathbf{r}_f - \mathbf{r}_i|}\right) \tag{10}$$

Here, the limitations of our *COILS* software are more significant, as one is keenly interested in accurately determining sample losses. Our software also is not capable of calculating the scalar electric potential Φ, which is due primarily to electric charge at the interfaces between discontinuities in electrical conductivity and permittivity. Hence, it is useful to complement our calculations with full-wave calculations using commercial software.

In *COILS*, a simplex algorithm determines the external shield currents such that the external field is minimized, and current distributions across coil conductor elements in the coil may be determined automatically by requiring perpendicular components of $\mathbf{B}_1$ to vanish near the surface of wide conductors or by minimizing inductance while holding total current constant. Recalculations (each iteration) on an 800 MHz Pentium-II typically take a few seconds to a minute, depending on the extent of the changes and the mesh sizes. A high level of confidence in this approach has been established from seven years of experience in successfully applying *COILS* to numerous gradient, susceptibility, and rf coil problems, as described in more detail elsewhere [*2, 8, 13, 35*]. With the macroscopic current distributions determined (typically to within ~2% of the coil diameter), Q_0 may be determined with sufficient accuracy from parametric relationships based on skin depth and the edge current density. The main reasons for wanting to know detailed current distributions are (a) to develop novel coil geometries that achieve high B_1 homogeneity with less reliance on precision phase shifts and (b) to optimize sensitivity – i.e., $\eta_F Q_L$.

For many cases, the calculation of the integral of $\sigma_E \boldsymbol{A} \bullet \boldsymbol{A}$ alone (where σ_E is the sample conductivity) gives an excellent approximation of the induced losses. For a cylindrically symmetric sample inside a cylindrically symmetric field for example, Φ vanishes within the sample. Our *COILS* software was recently shown to predict Q_0 and Q_L within 20% for complex 100 mm rf coils between 25 MHz and 300 MHz with uniform samples of salinity from 0 to 200 millimolar; and L and η_F are usually calculated within ~2% – a capability we have not seen in any other software.

Because of the potential to gain improved understanding of the behavior of the fields in both our linear and quadrature litz coils, we have been supporting collaborative simulation efforts at Hershey Medical Center (M. Smith, Q. Yang, J. Wang, C. Collins). They are beginning to simulate our SQT2 litz coil (see section 4.4 and Fig. 16) and will soon begin simulating our litzcage using XFDTD. We plan to purchase suitable 3D full-Maxwell software during the Phase II so that we can carry out such simulations in-house to complement the design capabilities of our proprietary software. We plan to evaluate at least three of the leading options (3DHFSS and Maxwell-3D by Ansoft; Fidelity from Bay Technology; ELECTRA by Vector Fields; XFDTD from Remcom; and MAFIA) before making a selection during Phase II.

4.3 Simulations of linear litz coils and birdcages. The simulations indicate σ_B is actually a little better for our linear litz coils than for a perfectly tuned 16 rung linear birdcage, and it is considerably better than that of the typical birdcage. Part of the reason is that the current densities in the end arcs are controlled and distributed in a more optimal manner. Again, even though filling factor for linear polarization is divided by two compared to circular, relative SNR – $(\eta_F Q_L)^{1/2}$ – of the 10 cm CFL2 coil at 70 MHz with a moderate load (8 cm diameter cylinder of 35 mM saline) was better than that of a quadrature birdcage used for comparison [*13*]. The primary reason for the improved S/N of this loaded linear litz coil appears to be that maximum axial rf magnetic field in the sample near the end edges is only one third as large as in birdcages. Hence, inductive loss in the sample (***dA/dt***) in this region is reduced. **Figure 13** (below, right) illustrates this in a color scale display of ***A•A*** (approximately E^2/ω^2) for one quadrant of the x=18 plane in a litz coil of 50 mm diameter. **Figure 12** (below, left) shows the same view for the linear birdcage. Note the much higher E field near the end ring and rung for the birdcage.

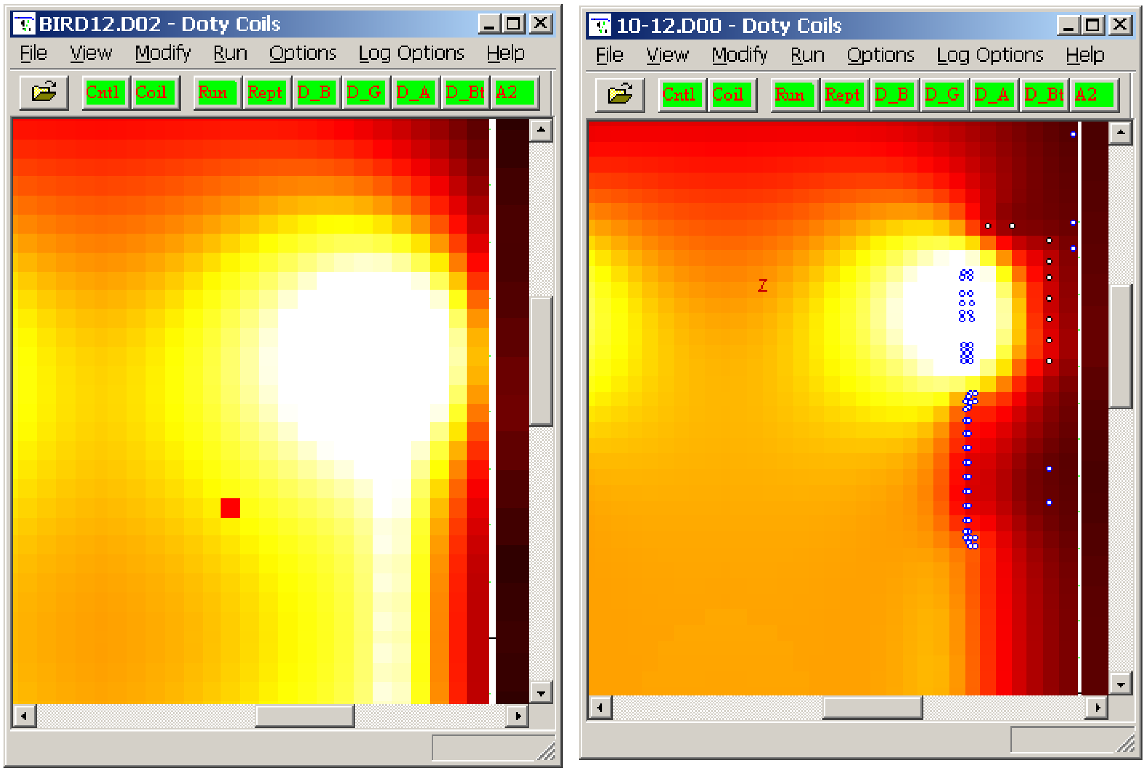

Figures 12 and 13. Color-scale display of ***A•A*** in the x=18 plane for a shielded litz coil (right) and a shielded birdcage (left). The two scales have been normalized to the same value at the center, and highest values are white. (There is a small gridding artifact near the edge of the sample region in the birdcage simulation.)

Excellent agreement has been obtained between measured and calculated data (Q_0, Q_L, σ_B, and η_F) in numerous experiments with linear litz coils fabricated from thin copper foil for numerous sizes and frequencies, some of which appear in the references [*2*, *13*, *36*] and may be readily compared to birdcage data for very similar conditions [*2, 37, 38*].

Of course, the CP birdcage has lower sample loss than the linear litz coil above some *fd*. But we generally obtain higher sensitivity and homogeneity with a *linear* litz coil than with a *quadrature* birdcage, for *fd* up to ~8 MHz-m for the larger coils and *fd* up to ~18 MHz-m for the smaller coils. **The primary point of the above discussion is to emphasize the need to more carefully investigate sample loss minimization in novel CP coils, as it is quite possible that equally unexpected discoveries will be made there.**

Below, we compare the results of simulations on the 8-rung birdcage, the Crozier 8/16 birdcage [*27*], the 16-rung birdcage, and the 8-section litzcage, all assumed to be perfectly symmetric. **Figures 14** and **15** (next page) illustrate the B_1 field in one quadrant of the z=2 cm plane for the 16-rung birdcage and 8-section litzcage respectively.

Table 1. Results from Simulations using *COILS* on Shielded 10 cm MRI Coils at 300 MHz

Coil Type	# of Capacitors	**σ_B, %** (8x6 cylinder)	η_F %	Q_0	Q_L	$\eta_F Q_L$ (S/N)
8-Rung BC	16	15.5	7.1	460	53	376
Crozier 8x2	16	12.9	6.4	470	59	378
16-Rung BC	32	9.4	7.2	470	52	375
Litzcage	16	9.9	6.5	480	58	377

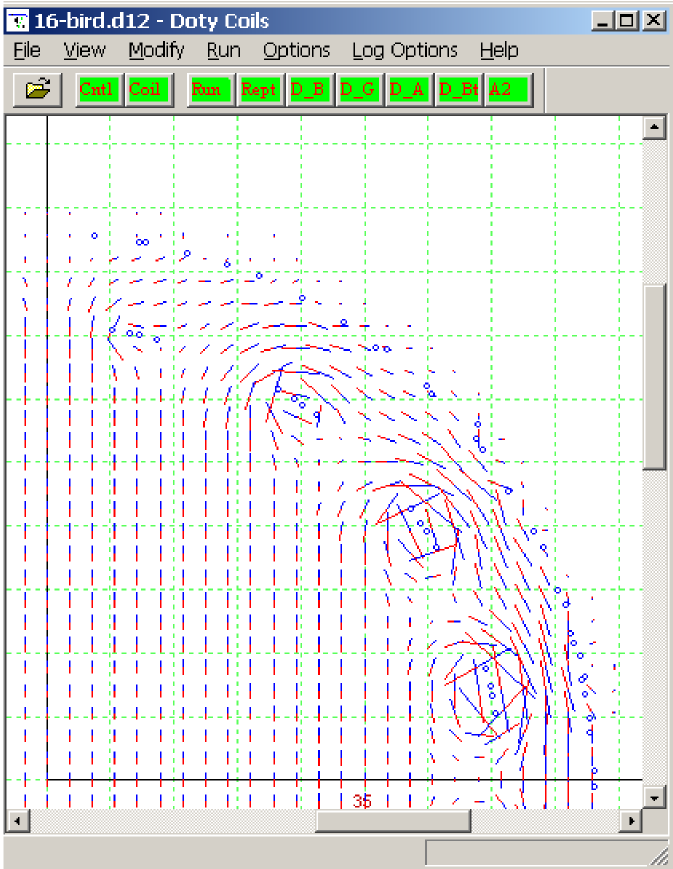

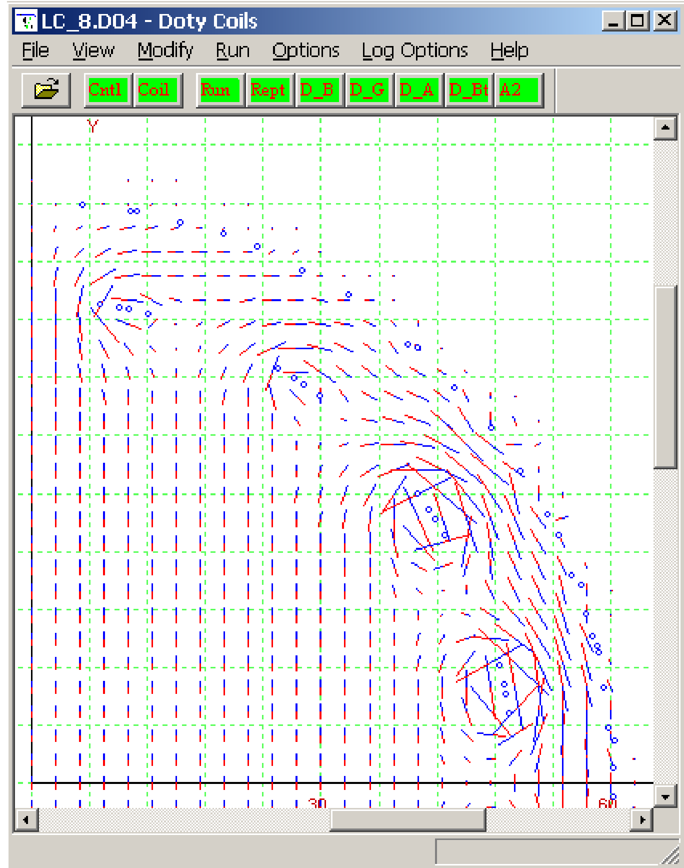

Figures 14 and 15 above display B_1 in the z=2 cm plane for the 16-rung birdcage and the 8-section litzcage.

4.4 Double-Resonance MRI at High-Fields using Orthogonal Linear Litz Coils. Quite a number of papers have appeared over the past decade presenting various coil designs for double-resonance MR. While positive aspects can be identified in all of these designs, they also each have their own set of disadvantages, as partially summarized in a recent paper [*38*]. For example, those utilizing alternate rungs for the separate frequencies have generally used 16 rungs total, 8 for each frequency. The homogeneity at either frequency is considerably worse than in an 8-rung single-resonance birdcage because (1) the rung width and spacing are very far from what would be optimum for an 8-rung birdcage to accommodate the 16 rungs, and (2) the reverse current flowing through the alternate rungs for the second frequency is not zero at the first frequency. While one can certainly achieve adequate homogeneity from an 8-rung single-resonance birdcage for a relatively small sample when the external shield is not too close, our simulations indicate it is unlikely that σ_B below 26% is possible for a sample diameter 70% of the coil diameter for *s*=1.2 in a 16-rung double-resonance high-field birdcage. The tuning difficulties make 24 rungs impractical for double-resonance. In fact, the tuning difficulties have led some to use 8 rungs total (4 per mode) and accept its severely degraded homogeneity and efficiency. A variation on the alternate-rung double-tuned birdcage is the alternate-rung double-tuned TEM resonator, which has been demonstrated at up to 4.1 T [*39*], but is very difficult to produce and tune to various samples because of the weaker couplings and closer mode structure, as noted earlier.

Some improvement in the alternate-rung birdcage is possible by employing a low-pass (LP) design with ^{1}H traps on the low-γ rungs [*38*]. Still, the coil is basically a poorly optimized unbalanced LP 8-rung birdcage at the ^{1}H frequency and hence has rather poor performance at 1.5 T and is probably not practical at 3 T.

Other approaches to double-resonance birdcages have been to extend a method used in double tuning single coils (in which the tuning capacitors are replaced with properly tuned traps) to both the low-pass and high-pass birdcages [*40, 41*]. This approach has proven to be both impractically difficult (even when space is not tightly constrained) and quite inefficient. Other approaches have used two concentric birdcages, two axially overlapping birdcages, or multiple-ring birdcages. All of these approaches, in addition to the tuning and coupling problems, generate non-overlapping B_1 regions at the separate frequencies, and hence have increased sample losses and considerable sacrifice in S/N compared to the optimum single-tuned coil. Some of the above drawbacks are exacerbated for the smaller microscopy coils, where the space external to the coil is more tightly constrained.

The approach we have shown to be more effective in the small to intermediate-size range (i.e., mice at 200 to 750 MHz, rats at 100 to 500 MHz, and a 25 cm coil at 1.5 T) is to use two orthogonal linear litz coils. The transparency of our litz coils to orthogonal flux makes it easier to achieve high homogeneity, maximum S/N, and greatly simplified

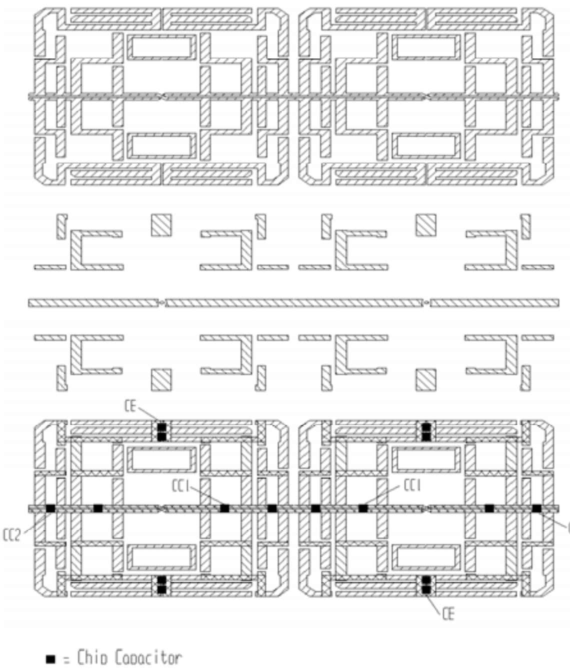

Figure 16. The SQT2 litz coil patterns.

tuning. Our ^{1}H/X coils for small animals tune quickly between ^{31}P, ^{13}C, ^{23}Na, and ^{17}O with almost no effect on the ^{1}H tuning.

Published, comparative data for double-resonance microscopy MRI coils is quite sparse, but in all small and intermediate-size cases where unambiguous comparisons can be made, we have seen dramatic advantages from our orthogonal-coil approach. For example, our 10 cm 200 MHz ^{1}H/X coil can be compared to data presented recently by a major manufacturer for a fixed-double-tuned 4-ring ^{1}H/^{13}C quadrature birdcage [*42*]. In this case, our coils achieve well over twice the S/N on both channels for a light load (mineral oil) and nearly twice the S/N on both channels for a heavy load (50 mM saline). Moreover, our coil achieves considerably better B_1 homogeneity and its multi-x channel tunes over a very broad range. Even stronger relative advantages (factors of 3) have been seen in our 32-55 mm ^{1}H/^{13}C probes at 4.7 to 11.8 T, as reported by our customers.

(We too find the above comparisons hard to believe, as our simulations do not suggest such a strong advantage for our coils – unless the birdcages have poor symmetry. The Varian 10 cm 200 MHz 4-ring ^{1}H/^{13}C coil reportedly required 500 W for ^{1}H pw90=120 μs and 1000 W for ^{13}C pw90=200 μs for a large cylinder of mineral oil. Our ^{1}H/X probe requires ~120 W for either of the above field strengths.)

The development of our second-generation Symmetric Quarter Turn (SQT2) litz coil, as shown in **Figure 16** was completed early in the Phase I and is now our most frequently used microscopy coil. It is consistently selected as the ^{1}H coil in our mouse and rat ^{1}H/X probes at 200-600 MHz. We also recently utilized this coil in a 25 cm ^{1}H/X probe for head studies on large non-human primates at 1.5 T, where the multi-X channel was tunable from ^{17}O to ^{31}P.

An unsegmented coil is required for the low-gamma coil for multi-nuclear tuning (^{31}P, ^{13}C, ^{17}O , ^{15}N) capability, but it is still necessary to have very low inductance and high homogeneity. Our Center-Fed One Turn (CF1T) coil shown in **Figure 17** represents a substantial improvement in coil technology for these applications [*15, 43*]. Essentially, it consists of two equal-inductance outer loops per side in parallel with a 2-turn inner coil on each side. A detailed analytical efficiency model was developed early in the Phase I for the single-tuned multi-nuclear CF1T coil with long leads and balanced tuning that allowed us to properly optimize the characteristics of the transmission line to the balanced, multi-nuclear tune/match network and accurately predict the tuning capacitor values, typically within ~2%. We also typically predict the rf field strength for a specified power and sample within ~12% over the full range of conditions (frequencies, sizes, samples) for which it is normally used.

Since most of the current flows in the four outer one-turn parallel loops, the total inductance of this coil is only ~10% more than that of the Kost (unsegmented) slotted resonator [*26*], but the region of high-homogeneity is increased from 65% to 85% of the coil diameter, so filling factor is increased by ~70%. Also, Q_0 is typically 20-30% higher. While it is most often used for the multi-x channel in mouse and rat ^{1}H/X probes, it has been used at up to 25 cm diameter and up to *fd* of 10 MHz-m. (A customer indicated its S/N on ^{17}O through ^{31}P was considerably better than had previously been obtained on quadrature birdcages on head studies in large non-human primates in a 25 cm coil at 1.5 T.)

We have had quite a number of inquiries from active researchers over the last two years concerning the availability of ^{1}H/X (28 cm) head coils for 2 and 3 T studies. The robust performance of the above mentioned 25 cm 1.5 T ^{1}H/X coil suggests that it will be rather easy to achieve similar performance in Phase II with these coils in a 28 cm coil for human head studies at 1.5 T and probably not too difficult at 2 T. However, it appears that it will be quite challenging to extend it to 3 T without major changes in both the ^{1}H and the multi-x coils. Several experiments were performed early in Phase I with a new litz coil pattern that has lower electric fields, especially near the ends

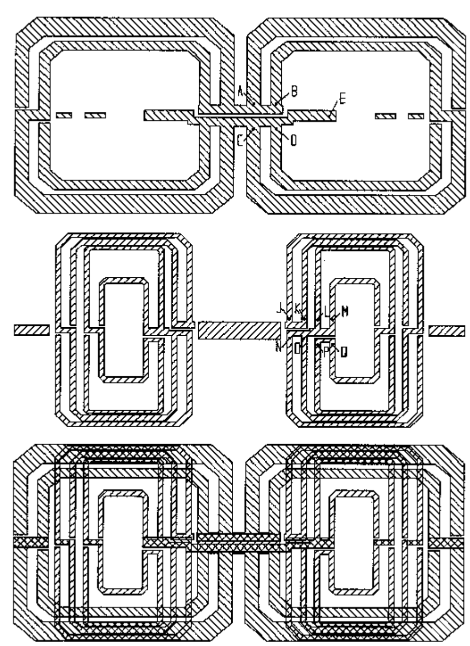

Figure 17. The CF1T multi-x foil patterns.

because of its higher-order symmetry and balanced end arcs. This new One-Sixth-Turn Balanced Arc Litz Coil (BAL6) is compatible with six segments around the B_1 axis. It has σ_B and η_F similar to that of the SQT2 coil, but its Q_0 and Q_L are both a little higher, and it appears to be usable at *fd* up to ~36 MHz-m.

Whether or not orthogonal linear litz coils will perform better than double-resonance birdcages in S/N for ^{1}H/^{31}P at 3 T on the human head is not yet clear. However, it does seem likely that B_1 homogeneity will be better and multi-nuclear tuning should be feasible, which is not possible with birdcages. Moreover, the tunability advantage of litz coils should permit enormous cost savings and greatly improved robustness, as we have consistently demonstrated with our smaller coils for animal research. (As noted earlier, our ^{1}H/X small-animal coils are typically priced at ~2/3 the price of those from our competitors *and* generally have more than twice the S/N on both channels.)

We plan to evaluate a 3 T ^{1}H/X coil based on orthogonal linear litz coils for human head MRI near the end of the first year of the Phase II effort. The ^{1}H coil will most likely be the BAL6, but a new linear litz coil will need to be developed for the multi-x channel. This coil will be similar to the CFL2 coil [*15*] in many respects but with more symmetric feed/tune features. We have not previously attempted multi-nuclear tuning of a litz coil above ~2/3 the *fd* product required here, so there could be some unexpected challenges. However, we have demonstrated the utility of symmetric center-fed tuning of half-turn litz coils and see no reason the methods cannot be made to work here.

The CP litzcage, as discussed next (which seems to be the ideal coil for single resonance with *fd* in the range of 10-100 MHz-m) should also have advantages in double-resonance head coils using alternate-rung concepts at 3 to 4 T. We plan to begin investigating that possibility near the end of Phase II.

4.5 Effect of Axial End Flux on Total Losses. There has been hope that further improvements in SNR would be possible by minimizing sample losses near the edges of the ROI by a careful optimization of the ratio of axial flux (from the ring currents) to transverse flux (from rung and ring currents). In the TEM coil, the axial end flux is minimized, as ring currents are minimal. While this may at first seem intuitively to be desirable (as it minimizes *L* and the rf magnetic field that is NMR inactive), the real goal for SNR is to minimize the integral of $\sigma_E \boldsymbol{A} \bullet \boldsymbol{A}$ *over the full sample space* (not just the ROI) relative to the integral of B_1^2 over the ROI. This appears to require *maximizing the rf gradient near the edges of the ROI*. In the birdcage with narrow rings, the relative axial fields are at maximum. Interestingly, the conventional birdcage and TEM coils appear to have nearly equal SNR when the various factors (rf mirrors, radiation, number of rungs, etc.) are similar (though the birdcage seems a little better [*22*]). This suggested the optimum lay between these two extremes.

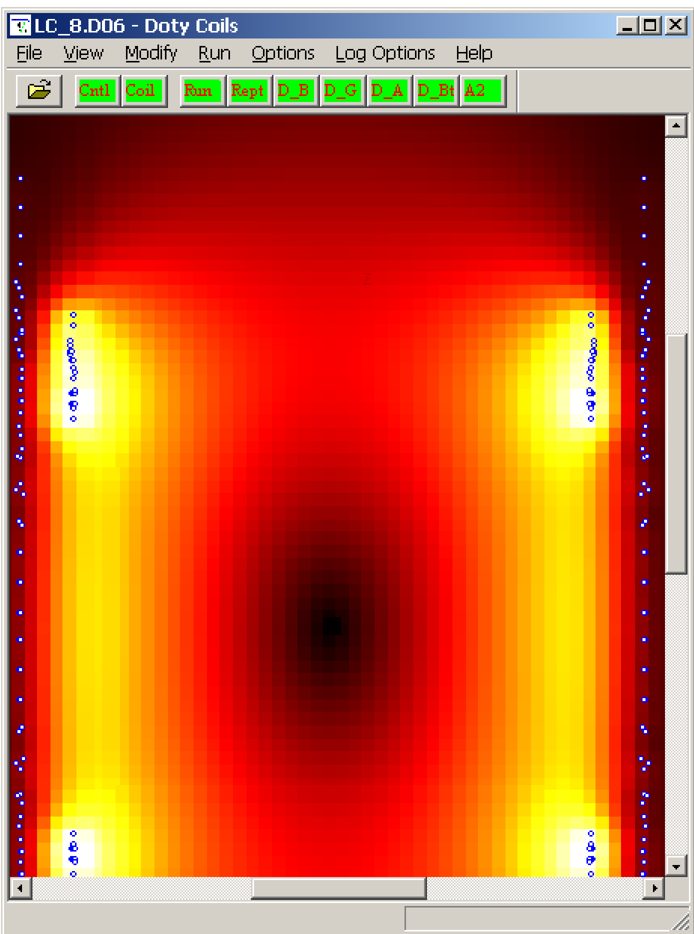

Figure 18. The A^2 field for the litzcage for the x=0 plane when B_1 is at 45^0 in the transverse plane (z is vertical). In CP mode, the SAR averages to approximately that shown here for constant sample conductivity at low dielectric constant. High-dielectric effects increase the central fields.

The relative axial end flux is determined primarily by (1) the ratio of shield diameter to coil diameter near the rings, (2) the relative width of the ring elements, and (3) the coil length to diameter ratio. Our simulations using *COILS* thus far on the effects of moving the rings radially closer to the shield while keeping the rungs in their initial location (moving the birdcage toward the TEM coil by suppressing axial end flux between the coil and shield) *has shown this change to be precisely neutral on S/N for the head-coil case*, where the patient body extends out one end of the coil; and it was very slightly detrimental in S/N for the case with only a central sample. Of course, there are errors from the dielectric effects, though it seems that these errors should be similar for the various coils, at least for the central region.

As previously noted, we have been supporting collaborative efforts at Hershey Medical Center aimed at simulating both linear litz coils and the litzcage using full-wave commercial software. But as of the time of this writing, we do not yet have conclusive results to report from those simulations.

It should be noted that while we are accurately calculating losses (coil and sample) for the long-wavelength case using our *COILS* software with cylindrically symmetric samples and fields, we are not simulating radiation (and neither are our collaborators using XFDTD). **Figure 18** (previous page) illustrates the $\boldsymbol{A}\bullet\boldsymbol{A}$ field for the litzcage of Figure 15 when B_1 is at 45^0 in the xy plane, which we believe to be close to the time-averaged SAR under CP conditions. Note that the maxima are at the edges, while the maxima for the B_1 field (which some have assumed to correlate to SAR) would be at the center.

It still seems to us that far-field radiation will be lower as the birdcage moves part-way toward the TEM, as this clearly reduces both the electric and magnetic dipole moments of the end arcuant elements, which are unarguably less efficient in generating transverse B_1. However, one study has reported end radiation from a well shielded birdcage head coil at 3 T to be insignificant [*22*]. Our preliminary simulations show a move in this direction permits a significant increase in filling factor (though not S/N, as Q_L would be reduced), which is tantamount to reducing inductance, and this allows the upper practical *fd* limit to be increased. (Interestingly, TEMs *as they have often been constructed* have lower η_F and higher Q_L, but that is not a requisite characteristic.) Clearly, this is an area that merits further and more complete simulations during Phase II that are not limited to the near field.

As mentioned previously, we propose to evaluate at least three existing commercial full-wave software packages for more accurate modeling of MRI rf coils. Some of the capabilities we will be looking for are to simultaneously simulate both the near-field and the far-field and to obtain accurate solutions reasonably quickly on standard desk-top computers (e.g., Athlon 1.8 GHz dual processor) under Windows 2000 or NT. Clearly, this requires more sophisticated meshing capabilities than we have seen in the FDTD software that we have had some experience with thus far.

4.6 Manipulating the External Conservative E field. As noted earlier in section 4.1, it is absolutely necessary that the individual element lengths not exceed $\sim\lambda_0/3$, and it has generally been assumed that smaller is better, as this reduces the conservative E fields emanating from both the conductor elements and the capacitors. One argument for the 8-section hybrid over the 16-section high-pass is that the longest element lengths in the 8-section hybrid are less than in the 16-section (or infinite-section, for that matter) high-pass. However, it is not obvious that one really wants to minimize the conservative E fields from the coil and capacitors. Rather the real goal is to minimize sample losses, given by the integral of $\sigma_E E^2$ over the sample. The total electric field **E** is given by

$$\mathbf{E} = -\partial\mathbf{A}/\partial t - \nabla\Phi_E, \qquad (11)$$

where Φ_E is the scalar electric potential due to electric charge, which may be concentrated, for example, at the interfaces between discontinuities in either the real or the imaginary component of the permittivity.

One method that has been used to reduce sample losses in non-living NMR samples (and in other related problems, such as transformer laminations) is to slice up the sample with insulating sheets. This has little effect on the first term in eq. (11) but drastically changes the second term in ways that completely alter the induced currents and reduce the losses. Of course, this is not an option for living samples, but it may be possible to alter the phase of Φ_E external to the sample in ways not previously considered so as to more effectively oppose $\partial\mathbf{A}/\partial t$ and reduce mean **E** within the sample. Our current software has not allowed us to investigate this possibility, but the full-wave software which we propose to acquire will. We have some specific ideas which we believe may be fruitful in reducing sample losses below what has been thought to be a theoretical limit, and they will be explored during Phase II.

4.7 High-order Passive and Active Shimming. The importance of high B_0 homogeneity in NMR is well appreciated. In low-field MRI the gradient strengths normally required for optimum resolution and S/N generally make the voxel separation more than twice the maximum chemical shift and large compared to B_0 perturbations from local variations in susceptibility. In high-field MRI, this condition may no longer be met, and shimming (homogenizing) the field becomes more important to reduce spatial errors, reduce shading, and improve spectral resolution.

Standard shim coils are designed to roughly approximate the magnetically orthogonal spherical harmonics over the full sample space (typically a 50 cm diameter of spherical volume (dsv) for whole-body magnets) to simplify homogenizing the field to the extent practical over the design dsv. However, there are serious limitations when shimming the head using whole-body shims for three reasons: (1) The near-field perturbations from susceptibility variations within the sample space cannot be fully corrected by any external shim coil system, however perfect it may be; (2) only the first and second-order shims are reasonably well-behaved and orthogonal for small sample volumes (such as the brain); and (3) while the linear shims have typical correction range of 10 ppm, the third-order gradients are generally limited to corrections of only ~2.5 ppm (Z^3 may have twice this range) at the surface of the design dsv, which means they (other than Z^3) would have a maximum correction of only ~0.3 ppm for a 25 cm dsv.

The primary sources of inhomogeneity in the head are the sinuses and nasal cavity, which unfortunately lie just below the brain. From the variation in susceptibility, one would expect the peak field inhomogeneities near these features to exceed 5 ppm. Passive shimming has been suggested as one possible avenue to improve homogeneity [*44*]. To explore several possibilities, we set up a crude susceptibility model using the method of effective surface currents [*35, 45*].

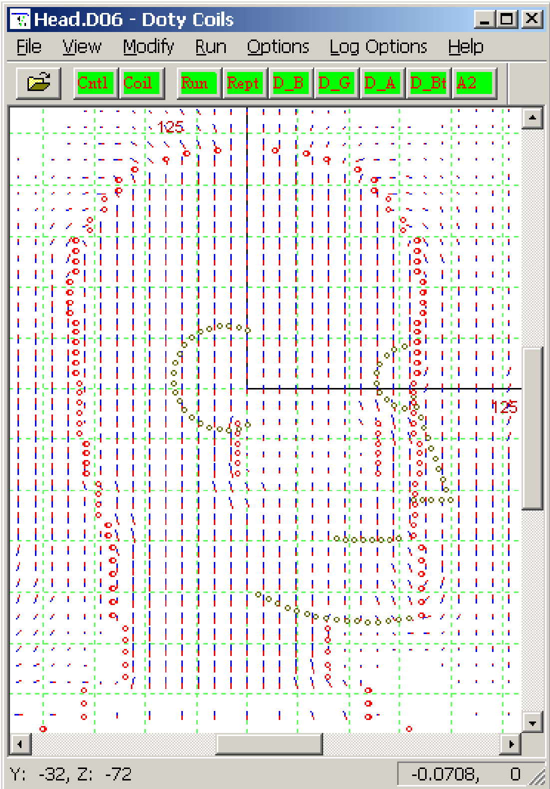

Figure 19. The field generated from the DC B_0 magnetization of the head after high-order shimming for best homogeneity throughout the upper brain. (The x=0 plane is displayed. The small circles illustrate **J** elements.)

The general solution for the surface current density $\mathbf{J}(r)$ at the boundary between two regions of uniform magnetization $\mathbf{M}_1$, $\mathbf{M}_2$ can be shown to be

$$\boldsymbol{J} = \boldsymbol{n} \times (\boldsymbol{M}_1 - \boldsymbol{M}_2) \qquad (12)$$

where **n** is the unit vector normal to the surface and directed from region 1 to region 2. It is straightforward to calculate effective surface currents for various simple geometries. For example, a uniform, solid paramagnetic or diamagnetic cylinder of susceptibility χ and length l aligned along the external field B_Z is equivalent to replacing the cylinder with a solenoid coincident with the cylindrical surface with ni ampturns, where

$$ni = \chi B_0 l/\mu_0. \qquad (13)$$

Likewise, it is easy to show that the current density on the outer surface of a long hollow cylinder is the same as for the solid cylinder, and the inner surface has an equal current density in the opposite direction. The surface currents on the plane faces at each end of the cylinder are zero.

Continuing in this way, we can accurately model complex 3D geometries using *COILS*. **Figure 19** illustrates the surface current elements in a sagittal plane for a simple model of the major susceptibility features of the human head, including the sinuses. The demagnetization field was calculated throughout the head for a uniform external B_0. In this case, the peak-to-peak field variation 10 mm above a large sinus cavity was calculated to be ~1.5 ppm, and the rms deviation in the region above the eyes was ~0.37 ppm (actually, within a half-ellipsoid approximating that portion of the brain above an axial plane through the eyes – positive z in Figure 19). The field was then (numerically) shimmed to the minimum linewidth throughout the upper brain using all first- and second-order shims (X, Y, Z, Z^2, X^2-Y^2, XY, ZX, and ZY) plus Z^3 and Z^4. The higher-order whole-body shims (X^3, Y^3, $Z(X^2$-$Y^2)$, XYZ, etc.) have insufficient strength for useful head shimming.

It is interesting to note that few users routinely shim beyond first order. This seems to be a significant limitation, as Z^2 was found to be the second most significant shim, and there are at least four (possibly six) non-linear shims more significant than X, assuming the magnet has been well shimmed and the rf coil is well designed.

There was little reduction in the peak-to-peak variations very near the sinuses, but the rms deviation throughout the half-ellipsoid was reduced to 0.13 ppm. We should point out that our method of approximating the sinuses in this preliminary model probably reduced apparent near-field variations by a factor of ~3, but the rms results throughout the 90% of the brain are reasonably valid. A more accurate model will be constructed during Phase II.

The order of significance of the shims from the perspective of linewidth improvement was as follows: Z, Z^2, Y, Z^3, X^2-Y^2, ZY, Z^4, XY, X, ZX. (Here, Y is in the posterior-anterior direction.) However, real (available) whole-body high-field Z^3, Z^4, and X^2-Y^2 shims probably have only two-thirds the range needed for full correction of the typical head, and practical Z^3 and Z^4 shims probably lack the purity needed for the small sample.

Two options are to increase the power and purity of the high-order shims, or include passive shims to assist in the mean high-order corrections. We have begun looking at both options. We are also currently in the process of developing a high-performance head gradient coil [*46*], and this gradient coil will include the primary non-linear shims with corrective ranges at least three times those typically found in whole-body shims. One might also initially suggest that a special shim-coil assembly could be made to slip over the rf coil and provide the additional needed range in the higher-order shims. However, this is not a complete solution because it is simply not possible to insure that the Z^3 shim coil (which is the second-most most important non-linear shim) will be sufficiently orthogonal (magnetically) to the Z-gradient coil to avoid huge eddy current problems. Both coils contain unspecified higher-order terms, and the Z^3 shim coil contains a substantial linear term outside its design dsv. For sufficient magnetic orthogonality of the Z^3 shim coil and the Z-gradient coil, the Z^3 coil must be specifically designed for the particular Z-gradient coil, and their relative winding locations must be very precisely controlled. **So two viable options are (1) a high-performance head-gradient coil with high-performance shims and (2) passive shims within the rf coil.**

A number of passive shims of both paramagnetic and diamagnetic materials have been evaluated with varying degrees of success. Thus far, we have restricted the evaluations to homogenizing the upper brain region because we do not have the post-processor needed to perform the linewidth analysis for arbitrary regions of space. We can analyze ellipsoids, or halves, quadrants, or octants thereof, so we have looked at the effects of passive shims only in the upper-half ellipsoid, as previously defined. A more general post-processor will be written during the Phase II to facilitate statistical analysis over the three quadrants of the ellipsoid that approximate the full brain and over arbitrary regions of space. (If the full-wave EM software we select for the 3D rf field simulations also happens to be well suited to magnetostatic problems, we may also find it useful here, but that will not be a significant consideration in the selection of the full-wave EM software, as *COILS* seems well suited for this magnetostatic problem.)

The most effective single passive shim seems to be a molded "beanie" cap of a soft polymer with an interior contour fitting that of the top of the head and an exterior hemispherical contour – i.e., a beanie cap that is thin at the edges and about 1-1.5 cm thick in the middle. This greatly reduces the Z^3 and Z^4 (and higher Z) shim requirements and reduces Z^2 a little. Polyethylene has susceptibility just 3% greater than that of water, but it is rather firm. Silicone rubber, being softer, would be more comfortable and could be loaded with a diamagnetic filler (such as alumina or magnesia powder) to present a good susceptibility match (and shorten T2). Either has sufficiently low dielectric constant and loss tangent and could easily be sterilized. Magnetically compensated silicone still has a long enough T2 to be faintly MRI visible under most conditions, but this should not be a problem. An assortment of several sizes would allow adequate fit for excellent high-order Z compensation of the full range of sizes of heads.

Some researchers have indicated that the rf mirror that is usually found in high-field rf coils provides some beneficial passive shimming if the mirror is backed by a thick (2-3 cm) plate of diamagnetic material (teflon, PMMA, etc.). Our simulations show the diamagnetic end plate primarily reduces Z shim current (which seems of no real benefit, as the Z-shim coils are never "max'd out") and helps Z^3 and Z^4 a little (depending on its thickness), but its help here is quite variable. The magnetically compensated cap seems to be a much better approach, and it does not require the coil to be closed at the top end (which would make the coil unusable for lower head and upper neck imaging).

The next most effective passive shim currently appears to be a throat pad. A small plastic bag (e.g., a sealed polyethylene sandwich bag) containing about a cup of water, resting on the throat, helps reduce ZY and $Z(X^2\text{-}Y^2)$ gradients. (With warm water, this is not at all uncomfortable.) We propose to evaluate both numerically and experimentally at 3 T the effects of several molded silicone beanie caps and throat pads on enhanced shimming during Phase II.

Teflon sectors may be placed in the space between the rf coil and its external rf shield to create some beneficial $X^2\text{-}Y^2$ and XY shimming above the sinuses. At this point it appears that it may be difficult to come up with an ideal solution for all patients, but we have just begun exploring the options. It seems likely that further explorations here during Phase II will yield a solution that provides useful enhancement without deleterious effects on the rf symmetry of the semi-open litzcage. We plan to include passive $X^2\text{-}Y^2$ (and possibly Y^3) shims in a head coil to be field tested during the Phase II. If adequate $X^2\text{-}Y^2$ passive shims can be incorporated into the semi-open rf coil, this combined with the magnetically compensated beanie cap and throat pad would enable full second-order and partial third- and fourth-order correction of the typical head with standard whole-body shim coils.

4.8 4-point-drive Litzcage Applications in Small Animal Models at 500 MHz. Despite their small size, the technical challenges of developing coils for research studies on mouse and rat models are considerable. Indeed, while the *fd* product for a 9 cm coil at 500 MHz is 20% less than that for a 28-cm head coil at 200 MHz, the former is likely to encounter loads ranging from 10% to 80% of its interior volume (and extending out both ends), while the latter will likely see loads ranging only from 15% to 25% of its interior volume. The technical challenges of small-animal volume coils are more analogous to those in human knee and whole-body coils than to human head coils. Hence, we expect our 4-point-drive litzcages to be particularly advantageous for small-animal volume coils at the highest fields.

During our Phase I, we began collaborations on mouse-head coils the Biomedical MR Laboratory (BMRL) at Washington University (St. Louis, MO), one of the original five US facilities funded through the NCI's Small Animal Imaging Research Program (SAIRP). A major ongoing challenge at the BMRL, as in other small-animal imaging research laboratories, is the development of state-of-the-art rf coils. The Washington University group has recently submitted an NIH grant to obtain a 500 MHz horizontal-bore imaging system, with a 12-14 cm clear-bore gradient system. While our linear CF1T litz coil performed better than the CP birdcage for mouse-head imaging (see Figure 2) at 200 MHz, the litzcage is clearly the preferred coil at higher fields or for samples larger than the mouse head at 200 MHz.

When the ROI is small, and especially if it is near the surface, there are certain advantages to using a volume coil for excitation and a surface coil for reception. For microscopy applications, the anesthetized animal must be securely restrained for accurate scan-to-scan registration and effective signal averaging. The experimental issues associated with the surface coil, anesthesia, animal handling, restraints, and life support are multiplied inside a small transmit coil. But a large transmit coil means more rf heating of the animal, so it is necessary that the transmit coil be quadrature for maximum flexibility in imaging techniques. Hence, the largest practical CP transmit coil is needed.

We plan to develop a robust CP 9.5 cm litzcage with active detuning for use inside a 12 cm clear-bore gradient system at 500 MHz. Four-point-drive is essential for such a coil to perform well over a wide range of loads, and active detuning is required for satisfactory operation of a CP coil with a surface coil. It is not yet clear whether the high-pass or the band-pass will be better suited here, nor is it clear which 4-point-drive balancing circuit or which method of active detuning will be best. However, it *is* clear that implementing all of this inside the tight radial space will be challenging. At this point, it appears we will need to add a fourth ring (opposite the tune end) to accommodate a balanced PIN-diode detuning bias network.

Some success has recently been reported with small-animal HP birdcage models based on coupled transmission lines at low *fd* products (<12 MHz-m) [*47*], and our partial successes with related models at higher *fd* suggest a robust solution for the hybrid litzcage for *fd* up to ~100 MHz-m can be developed. The 9.5 cm 500 MHz small-animal coil seems to be an ideal place to begin to work out the challenges of the hybrid litzcage with advanced four-point-drive balancing networks suitable for the most challenging MRI coils of the next decade.

4.9 Fabrication and Field Testing – Collaborations with Hershey Medical Center and Washington Univ.

As we have produced several coils previously for human research applications (including wrist and knee) and numerous mouse and rat coils, we will not devote much space here to fabrication and product development, but more details are included later in the section on Product Development. We should emphasize that we have a strong record of getting new products to market, and this will be a major and early priority during the Phase II.

Since we do not have a large magnet at DotyNMR, collaborations with other groups are essential. The group at Hershey Medical Center (Hershey, PA) combine a healthy balance of clinical imaging and high-field MRI research. They have been at the forefront of full-wave rf coil simulations and high-field applications for at least five years [*9*]. During the Phase I, progress was made in the simulations of our linear SQT2 litz coil, and valuable imaging experience was acquired with this coil (see Fig. 1). We plan to extend the scope of their simulations during Phase II to the circular polarization litzcage and compare their results to those we plan to obtain with the 3D full-wave software we propose to acquire under the Phase II. This is expected to require our support of a post-doc (possibly Dr. Jinghua Wang) at Hershey Medical Center for two years plus some overhead.

Perhaps more importantly, we plan to furnish four 3T coils to Hershey Medical Center for thorough field testing and evaluation during the coarse of the Phase II: a CP ^{1}H semi-open (litzcage) head coil, a CP ^{1}H semi-open (litzcage) knee coil, a double-tuned (perhaps ^{1}H/^{23}Na, probably linear) head coil, and a CP ^{1}H (litzcage) torso coil. Developing and productizing these advanced coils (other than the 3 T ^{1}H head coil) will be quite challenging, so it is likely that several iterations will be required. While some of the testing will be handled by the post-doc, some assistance from senior scientist Dr. Michael Smith and Dr. Qing Yang, Assistant Professor of Radiology, will also be needed here.

As noted earlier, we have established a collaboration with the NCI-funded BMRL at Washington University in the area of coils for high-field research on small animals at 200 MHz. The BMRL currently supports two 4.7T small-animal scanners and anticipates acquiring a 500 MHz horizontal-bore imaging system soon. The Washington University group has enormous experience in animal handling for MRI and we propose to further develop robust, fully open CP litzcages with user-friendly animal constraints under their guidance. We plan to supply their laboratory with a small-animal 200 MHz litzcage during the third month of the Phase II, and a large 500 MHz litzcage during the second year. We expect that senior BMRL scientist Dr. Joel Garbow will perform the majority of the testing and evaluation.

4.99 Conclusion

The primary overall Phase II objective is to permit a substantial increase in MRI patient throughput (thereby reducing scan costs) via relatively inexpensive upgrades of robust knee, head, torso, neck, and wrist rf coils in existing high-field MRI scanners.

The unique ability of our 4-point-drive semi-open CP litzcages to easily match to widely varying conditions reduces manufacturing costs and permits much more rapid tune up by the user, thus enabling improved utilization of MRI equipment. While this is beneficial for head coils at 3 T and higher, it is actually most significant for the knee and torso, as here the coils must have much higher η_F (either to limit losses outside the ROI or because of external space constraints), and this necessarily increases the variability in the loading effects.

Novel methods being developed for passive shimming of the B_0 field in head MRI are expected to be particularly beneficial in reducing image artifacts in fMRI methods such as EPI. Moreover, the ability of our axially asymmetric coil design to perform optimally without an end mirror not only greatly enhances the openness of the head coil, it also increases its flexibility, as it may also be used to image the lower head and neck.

In addition to completing the development of quadrature litz coils with improved tunability, S/N, and B_1 homogeneity at 3 T and 4 T for human head, knee, neck, and torso and for small animals at 4.7-12 T during this Phase II, we will also explore novel approaches to reducing those losses heretofore considered to limit the ultimate achievable SNR – those arising from the time derivative of the **A** vector in a homogeneous B_1. We hope to show that it will be possible in many cases to take advantage of sample dielectric resonances and externally created **E** fields (that would not be minimized, but would be properly phased, opposing the **A** field) so as achieve higher S/N than has generally been thought possible.

Field testing of a 3 T ^{1}H CP head coil, a 3 T CP knee coil, and a 4.7 T small-animal CP coil will begin very early in Phase II at the Hershey Medical Center, Hershey, PA and at the SAIRP at Washington University, MO. Field testing of a 3 T torso coil and a double-tuned ^{1}H/X head coil are planned for the second year. The FDA approval process for head, knee, wrist, and neck coils will begin during the Phase II.

5.0 Human Subjects. No experiments on humans will be performed at Doty Scientific under this grant. Field tests of the head, knee, neck, and torso coils will be carried out under the direction of Dr. Mike Smith and/or Dr. Qing Yang at Hershey Medical Center, Hershey, PA. These experiments will be non-invasive MRI on volunteers using established, approved protocols. Doty Scientific will furnish the group at Hershey Medical Center with SAR maps based on detailed simulations, field strength calculations, and bench test data on phantoms along with detailed tuning instructions with each coil furnished for evaluation.

6.0 Vertebrate animals. No experiments with animals will be performed at Doty Scientific under this grant. Field tests of the 500 MHz small-animal coils will be carried out at the BMRL at Washington University under the direction of Dr. Joel Garbow. The experiments will be non-invasive, microscopy MRI performed on anesthetized mice and rats in their laboratories using established, approved protocols. No animals will be sacrificed, and no additional animals will be needed for the evaluation of the small-animal MRI coils being developed and tested under this proposed grant. Doty Scientific will furnish the group at Washington University with SAR maps based on detailed simulations, field strength calculations, and bench test data on phantoms along with detailed tuning instructions with each coil furnished for evaluation.

7.0 References

1. *Clinical MRI,* 2nd ed., editors Edelman, Hesselink, Zlatkin, Saunders; Chapter 1, R. M. Weisskoff and R. R. Edelman, "Basic Principles of MRI", 3-51, 1996.
2. **F. David Doty**, **George Entzminger**, C. Hauck, and **John P. Staab**, "Practical Aspects of Birdcage Coils," *J. Magn. Reson.*, 138:144-154, 1999.
3. J. T. Vaughan, H. P. Hetherington, J. O. Otu, J. W. Pan, and G. M. Pohost, "High Frequency Volume Coils for Clinical NMR Imaging and Spectroscopy," *Magn. Reson. in Med.*, 32:206-218, 1994.
4. P. J. Ledden, L. L. Wald, and J. T. Vaughan, "A Four-Port-Drive Flat-Element Transmission-Line Coil for Brain Imaging at 3T," 8th ISMRM Conf., Poster #1395, Denver, 2000.
5. C. E. Hayes, W. A. Edelstein, J. F. Schenck, O. M. Mueller, and M. Eash, "An Efficient Highly Homogeneous Radiofrequency Coil for Whole-Body NMR Imaging at 1.5 T," *J. Magn. Reson.*, 63:622-8,1985.
6. H. Merkle, W. Driesel, P. Andersen, G. Adriany, K. Ugurbil and M. Garwood, "Circularly Polarized RF Helmet Coil for Brain Studies at 7 T," 8th ISMRM Conf., Poster #565, Denver, 2000.
7. D. L. Price, J. P. DeWilde, A. M. Papadaki, J. S. Curran, and R. I. Kitney, "Investigatin of Acoustic Noise on 15 MRI Scanners from 0.2 T to 3 T," *JMRI*, 13:288-293, 2001.
8. **F. David Doty**, "Optimization of MRI Gradient Coils" in *Spatially Resolved Magnetic Resonance*, Ed. by P. Blumler, B. Blumich, R. E. Botto, and E. Fukushima, Wiley-VCH, Weinheim, 1998.
9. C. M. Collins, S. Li, Q. X. Yang, and M. B. Smith, "A Method for Accurate Calculation of B_1 Fields in Three Dimensions. Effects of Shield Geometry on Field Strength and Homogeneity in the Birdcage Coil," *J. Magn. Reson.*, 125:233-241, 1997.
10. O. Ocali and E. Atalar, "Ultimate Intrinsic Signal-to-Noise Ratio in MRI," *Magn. Reson. in Med.*, 39:462-473, 1998.
11. G. Glover, C. Hayes, N. Pelc, W. Edelstein, O. Mueller, H. Hart, C. Hardy, M. O'Donnell, and W. Barber, "Comparison of Linear and Circular Polarization for Magnetic Resonance Imaging," *J. Magn. Reson.*, 64:225-270, 1985.
12. E. A. Barberi, J. S. Gati, Brian K. Rutt, and R. S. Menon, "A Transmit-Only/Receive-Only (TORO) RF System for High-FIeld MRI/MRS Applications," *Magn. Reson. in Med.*, 43:284-289, 2000.
13. **F. David Doty, George Entzminger Jr**, and Cory D. Hauck, "Error-Tolerant RF Litz Coils for NMR/MRI", J. Magn. Reson., 140:17-31, 1999.
14. G. Adriany, E. Yacoub, I. Tkac, P. Andersen, H. Merkle, J. T. Vaughan, and K. Ugurbil, "Shielded Surface Coils and ... Resonators ... at 7 T," 8th ISMRM Conf., Poster #563, Denver, 2000.
15. **F. David Doty**, "Low Inductance Transverse Litz Foil Coils," US Pat # 6,060,882 (2000).
16. D. K. Spence and S. M. Wright, "An Efficient Model for Evaluating the Effects of Leg Current Distributions on Birdcage Coils," 8th ISMRM Conf., Poster #1397, Denver, 2000.
17. F. Hwang, D. I. Hoult, "Automatic Probe Tuning and Matching," *MRM.*, 1998, 39:214-222.
18. J. B. Miller, B. H. Suits, A. N. Garroway, and M. A. Hepp, "..Recovery Time, Signal, and Noise.." *Concepts in Magn. Reson*., 1999.

19. J. Tropp, "The Theory of an Arbitrarily Perturbed Bird-Cage Resonator, and a Simple Method for Restoring It to Full Symmetry," *J. Magn. Reson.,* 95:235-43, 1991.
20. J. M. Jin and J. Chen, "On the SAR and Field Inhomogeneity of Birdcage Coils Loaded with the Human Head," *Magn. Reson. Med.*, 38:953-963, 1997.
21. R. Hurd, GE Medical Systems, private communication, 4/2000.
22. J. Tropp and P. Calderon, "Direct Comparison of Transmit Efficiency in Birdcage and TEM Resonators," presented at ISMRM, Glasgow, Scotland, 2001.
23. J. Tropp, "A Model for Image Shading in Multi-mode Resonators," presented at ISMRM, Glasgow, Scotland, 2001.
24. P. B. Roemer, W. A. Edelstein, C. E. Hayes, S. P. Souza, O. M. Mueller, "The Phased Array," *Magn. Reson. Med*. 1990; 16:192-225.
25. D. W. Alderman and D. M. Grant, "An Efficient Decoupler Coil Design which Reduces Heating in Conductive Samples in Superconducting Spectrometers," *J. Magn. Reson.*, 36:447-51,1979.
26. G. J. Kost, S. E. Anderson, G. B. Matson, and C. B. Conboy, "A Cylindrical-Window NMR Probe ... for Studies of the Developing Heart," *J. Magn. Reson.*, 82:238-52, 1989.
27. S. Crozier, D. M. Doddrell, "RF Resonator for NMR," US Pat #5,642,048, 1997, U. Queensland.
28. J. Jin, *Electromagnetic Analysis and Design in MRI*, CRC Press, Boca Raton, 1999
29. J. S. Tropp, "Mutual Inductance in the BirdCage Resonator," *J. Magn. Reson.*, 1997; 126:9-17.
30. V. J. Sank, C-N. Chen, and D. I. Hoult, "A Quadrature Coil for the Adult Human Head," *J. Magn. Reson.*, 1986, 69, 236-242.
31. T. S. Ibrahim, R. Lee, B. A. Baertlein, and P. M. L. Robitaille, "Obtaining a Homogeneous B_1 Field at UHF: Use of Multiple Drives and Variable Amplitude/Phases," presented at ISMRM, Glasgow, Scotland, 2001.
32. C. M. Collins and M. B. Smith, "SNR and Absorbed Power as Functions of Main Magnetic Field Strength, and Definition of "90^0" RF Pulse for the Head in the Birdcage Coil," *Magn. Reson. Med.,* 45, 684-691, 2001.
33. J. T. Vaughan, M. Garwood, C. M. Collins, W. Liu, L. DelaBarre, G. Adriany, P. Andersen, H. Merkle, R. Groebel, M. B. Smith, and K. Ugurbil, "7T vs. 4T: RF Power, Homogeneity, and Signal-to-Noise Comparision in Head Images," *Magn. Reson. in Med.*, 46, 24-30, 2001.
34. P. M. Joseph and M. Saadi-Elmandjra, "Electrical Field Measurement in Cylindrical Imaging Coils," J. Magn. Reson., 1987, 75, 199-212.
35. **F. David Doty**, **G. Entzminger**, Y. Andy Yang, "Magnetism in High-Resolution NMR Probe Design. I: General Methods," *Concepts in Magn. Reson.*, **10**(3) 1998, 133-156.
36. S. Sukumar, "EPI on High Field Microscopy Systems," *Magnetic Moments* 8, 4, 13-16, 1997.
37. Mark C. Leifer, "Theory of the Quadrature Elliptic Birdcage Coil," *MRM*, 1997, 38:767-732.
38. Matson GB, Vermathen P, and Hill TC, A Practical Double-Tuned $^1H/^{31}P$ Quadrature Birdcage Headcoil Optimized for ^{31}P Operation, *J. Magn. Reson.,* 1999:139:81-89.
39. J. T. Vaughan, H. P. Hetherington, G. M. Pohost, "Multiply Tuned, High Frequency Volume Coils for Clinical NMR," proc. 12th SMRM, p. 306, NY, 1993.
40. J. R. Fitzsimmons, H. R. Brooker, and B. Beck, "A Comparison of Double-Tuned Surface Coils," *Magn. Reson. in Med.*, 1989, **10**, 302-309.
41. G. X. Shen, J. F. Wu, F. E. Boada, K. R. Thulborn, "...Dual-Tuned, Low-Pass Birdcage... for MRI and MRS of Human Brain at 3.0 Tesla", *Magn. Reson. Med.,* 1999; 41:268-275.
42. (E.) W. H. Wang, S. Sukumar, and H. Hill, "Design and Evaluation of Double-Tuned Birdcage Coils," presented at 40^{th} ENC, poster #211, Orlando, FL, 1999.
43. **F. D. Doty** and **G. Entzminger Jr**, "Center-fed Paralleled Saddle Coils for Multinuclear Double-Resonance NMR or MRI," US patent # 6,175,237.
44. M. Smith, Q. Yang, "Correction of Local Field Distortion in High Field MRI," ENC, Asilomar, 2000.
45. T. M. Barbara, "Cylindrical Demagnetization Fields and Microprobe Design in High-Resolution NMR," *J. Magn. Reson. Ser. A*, 1994, 109, 265-69.
46. **F. D. Doty**, “A Quite, High-Performance, High-Field MRI Gradient Coil,” current Phase I NIH SBIR grant, 1 R43 NS41127-01.
47. P. J. Cassidy, S. Grieve, K. Clarke, D. J. Edwards, "Electromagnetic Characterisation of RF Coils Using the Transmission Line Modeling (TLM) Method," presented at ISMRM, Glasgow, Scotland, 2001.
48. **F. D. Doty**, "Solid State NMR Probe Design," *The Encycl. of NMR Vol. 7*, Wiley, 4475-4485, 1996.

49. R. Bowtell and P. Mansfield, "Quiet Transverse Gradient Coils: Lorentz Force Balanced Designs Using Geometrical Similitude," *Magn. Reson. in Med.*, 34, 494-97, 1995.

8.0 Consultants and Subcontractors

Dr. Michael B. Smith, Department of Radiology/NMR Bldg. Penn. State College of Medicine, Hershey, PA will consult on matters related to requirements and performance of MRI rf coils for clinical and human research applications at high fields. Dr. Joel Garbow, Biomedical MR Laboratory, Washington University School of Medicine, Washington University, will consult on matters related to animal handling, life support, and experimental requirements for MRI rf coils for animal research applications at high fields. Each of these researchers is requesting funding for the portions of the research and testing that will be performed at their respective facilities.

9.0 Product Development Plan

9.1 Relevant NMR/MRI Instrumentation and RF Coil Experience. Doty Scientific's historical focus has been on specialized probes and coils for NMR and MRI. We have been developing and producing custom, precision RF and electro-mechanical instruments, primarily for research in solid-state NMR, for nearly 20 years and are the recognized world leader in these specialties. About half of our customers are University Chemistry Departments, and the balance are primarily industrial research labs. About 30% of our sales are international – mainly to the UK, Japan, Canada, and Germany, but we have products in at least 20 countries.

Over 90% of our developments have been totally funded by profits from sales of products. We are truly a customer-driven developer and producer of sophisticated, customized products for world-class scientists (including several Nobel laureates) and engineers. Often we offer new technical capabilities that we have not previously delivered – and we virtually always come through. Fewer than 0.5% of our products are returned for refund.

The NMR probe industry has been rather competitive and very fast paced for the past decade. For a small business to maintain an adequate market share in this environment, new products must be introduced annually. In many cases, our advances occurred incrementally and with primary focus on a particularly capability; but four times over just the past seven years we have introduced new solids NMR spectroscopy probes with major advances in numerous specifications simultaneously. These achievements have required an exceptional level of creativity, motivation, and technical skill at all levels and provide constant challenge to our staff, currently of 37 full-time equivalents, including 3 PhD scientists, 6 MS engineers, and 12 BS-level scientists and engineers. Fifteen of our employees have been with the company for more than seven years, and eight for more than 13 years.

Although initially known to specialize in solids NMR, some of the technological improvements there led us more into the related technology of MRI rf coils about 8 years ago. Within the past year, it has become clear that our radically new approach to efficient, homogeneous rf coil design will soon be recognized as having enormous significance for double resonance MRI at high fields [*13*]. Here, we typically obtain more than twice the rf efficiency on both channels compared to alternative approaches, and experiments in a number of labs demonstrate other strong advantages. These double-resonance, multi-nuclear MRI volume coils (for example, capable of $^{1}H/^{31}P$ and $^{1}H/^{23}Na$ in the same probe) are often included with our mice and rat gradient coils [*36*]. These developments would not have been possible without our unique software developments in electromagnetic field simulations [*2, 8, 13, 15*].

We recently completed a multi-nuclear rf coil for 1.5 T brain research on large, non-human primates at the University of Chicago. This single unit (utilizing two orthogonal linear litz coils) is capable of the following double-resonance experiments at 1.5 T: $^{1}H/^{31}P$; $^{1}H/^{13}C$; $^{1}H/^{23}Na$; and $^{1}H/^{17}O$. It is also capable of ^{31}P, ^{23}Na, ^{13}C, and ^{17}O spectroscopy at 3 T. Moreover, in addition to its enormous advantages in ease of use, it achieved considerably higher S/N on the multi-X channel than was obtained on the prior quadrature birdcage of similar size at 1.5 T. Additional product information and litz-coil images may be found at www.dotynmr.com.

9.2 Related Products and R&D. Over the past six years, we have made a number of major advances in solids NMR spectroscopy probes. For example, one of our major products provides high-speed Magic Angle sample Spinning (MAS) of solid samples to improve spectral resolution [*48*]. Twelve years ago, our ability to spin 5-mm NMR solids samples at rates of 9 kHz with double-resonance rf circuitry capable of rf field strengths of 20 G at 300 MHz (requiring ~2.5 kV) was considered phenomenal. Today, to succeed against large, well-financed competitors, our MAS products must exceed our competitor's specifications in all respects by at least 30%. That means we have to spin 4 mm samples at 26 kHz (>1.5 million rpm), generate 30 G fields at 800 MHz, accommodate a wider range of sample temperatures, minimize more NMR background signals, and achieve higher rf sensitivity in a triple-resonance probe inside a narrow-bore 20 T magnet – and all of these capabilities in the same product. Further advances in fast MAS

NMR technology for improved determination of molecular structure in biological macromolecules is the subject of a currently supported Phase I SBIR, 1R43RR16417-01.

It has been about 16 years since Doty Scientific Inc (DSI or *DotyNMR*) shipped the first commercially available shielded gradient coil for high-field microscopy. Three different sizes (for rat, mouse, and even smaller samples) of the initial design were produced for several years before it became clear that it was imperative to address coil vibration and acoustic noise more effectively by winding gradient coils that permitted accurate force-cancellation between oppositely directed current elements with minimal axial separation. During the next several years, the crescent gradient coil design evolved [*8*], and shipping began for mouse MRI microscopy in 1993. (Later, a number of other research groups, most notably Mansfield's [*49*], published related designs that also achieved some noise reduction, but with severe penalties in efficiencies [*8*].) For the past 8 years, Doty Scientific has produced gradient coils for mouse and rat microscopy at ultra high fields with unmatched reliability and performance. While the marketing strength of several large competitors (especially Varian and Bruker) has limited our commercial success in this niche market, there are recent indications that our MRI gradient coil technology may see increased commercial success. GE has recently expressed serious interest in our gradient coil approach for whole body gradients.

9.3 Prior Funding Successes. Some of our other related products include double- and triple-resonance MRI surface coils and low-noise rf pre-amps, some of which were developed under a Phase II SBIR, NIH #44-CM-77804, in 1987. A Phase I SBIR [1 R43 NS41127-01] is currently supported by NIH for the development of a high-performance, quiet, MRI head gradient coil that could be used with the rf coil proposed herein [*46*].

The development of the new products that Doty Scientific offers has been primarily financed through in house funding. This is true also of the technological advances in existing products. Our most recently funded Phase II project (DOE DE-FG02-98ER82565) – “Development of 1-10 W, 10 K Reverse Brayton Cycle Cryocoolers” has yet to result in any commercial products. However, work is continuing, and commercial products are expected here for cryogenic and power generations applications within a year.

9.4 Some MRI RF Coil Manufacturing Considerations. As we have produced several coils previously for human research applications (including wrist and knee) and numerous mouse and rat coils, we will not devote much space here to manufacturing. However, we should note that we are proposing a very ambitious Phase II that, in addition to the programming, simulations, and theoretical work discussed earlier, will include the detailed development, fabrication, and testing of at least four very challenging coils: (1) a 3 T CP ^{1}H semi-open knee coil, (2) a double-tuned (perhaps ^{1}H/^{23}Na, probably linear) 3 T head coil, (4) a 500 MHz actively detuned 9.5 cm CP small-animal coil, and (4) a CP ^{1}H torso coil. Of course, we will complete the development and testing of the passively shimmed, semi-open, easily tunable, CP, ^{1}H 3 and 4T head coils that were the focus of the Phase I effort, but that is not expected to be very challenging at this point – though sufficient attention must be paid to productizing issues.

Figure 20 Photo showing the litzcage and tuning elements on the semi-open coilform.

Some appreciation for the potential for cost reduction is clear from the simplicity of the design, as is apparent in the photo of **Figure 20** showing the litzcage and tuning capacitors mounted on the windowed coilform. The litzcage is the simple product of a photolithographic etching procedure rather than an assembly of precision-manufactured coaxial resonators, for example. Determining the optimal procedure for producing these coils in quantity will be investigated

In all cases, both the shield and coil elements will be capacitively segmented so that gradient eddy currents and rf electric fields within the sample are sufficiently minimized [*8, 36*]. Coilform materials in regions of high B_1 will be non-hydrogenous (Teflon, Kel-f, ceramic, etc.) to the extent practical and otherwise of highly rigid polymers with minimal T2, high chemical stability, and sufficient flame retardance (polyetherimides, composites, polycarbonate) for regulatory requirements.

For the semi-open coils (the CP head and knee coils), the optical windows through the shield/coil slots will be framed and sealed to maintain adequate moisture resistance of the coil. High-reliability rf capacitors with sufficient voltage breakdown margins will be used [*48*]. Proper attention will be paid to cuts in the shield and coilform near the ROI to minimize B_0 susceptibility artifacts [*35*]. The outside diameter will be under 36 cm for compatibility with most head gradient coils, including one we are developing. The inside will be lined with foamed Teflon. The prototypes will be assembled from components fabricated from stock tubing and sheet materials, as in Phase I, but the productized versions may utilize injection-molded external covers.

9.5 Bench Testing. Bench tests will begin with relative B_1 field mapping and measurements of η_F, Q_0 and Q_L, for the full range of typical loads. S/N will be evaluated by comparing the τ_{90} efficiency to that for other published data. The experimental data will be compared to the numerical simulations, as described earlier. Tuning ranges and effects of tuning and asymmetric loads on σ_B will be documented and compared to the simulations. High-power rf testing will be performed, as will tests of rf tuning stability, mechanical integrity, experimental verifications of rf power deposition, and B_0 passive shimming calculations. The 3T CP ^{1}H head coil will be ready for field-testing within the first month of the Phase II. The 3T CP ^{1}H knee coil and a 200 MHz small-animal coil will be ready for field-testing during the third month. The double-tuned 3 T head coil will be ready for testing late in the first year, and the 3T torso coil and 500 MHz small-animal coil will be ready for testing early in the second year. Testing of the Head and Torso coils will be performed under the supervision of Dr. Michael Smith at Penn State School of Medicine / Hershey Medical Center. The small animal coil will be tested on mice and rats under the supervision of Dr. Joel Garbow at the Washington University School of Medicine.

9.6 FDA Approval for Clinical MRI. Our RF coil, specifically the 3T CP ^{1}H Head Coil which will be the initial product, is identified as a magnetic resonance diagnostic device. Its classification is a Class II Medical Device in accordance with the Code of Federal Regulations, Title 21 Chapter I Part 892 Subpart B Section 892.1000. Since the coil is a Class II device, premarket approval (PMA) is not required. This type of device, however, is not exempted from premarket notification [510(k)] that must be filed per the FD&C Act. The format for 510(k) submission is detailed in 21 CFR 807 and it must be filed with the FDA at least 90 days prior to marketing the device. The purpose of the premarket notification is to establish the coil as “substantially equivalent” (SE) to a current, legally marketed (predicate) device.

A device is SE to a predicate device if they share the same intended use **and** have the same technological characteristics **or** different technological characteristics that do not raise new questions of safety and effectiveness. Until the FDA declares the device to be SE, we cannot market the coil. Class II devices are subject to the FDA’s general controls (applicable to all device classes) and special controls for class II devices.

General Controls include the provisions of the FD&C Act pertaining to: (a) Adulteration, (b) Misbranding, (c) Device registration and listing, (d) Premarket notification, (e) Banned devices, (f) Notification and repair, replacement, and refund, (g) Records and reports, (h) Restricted devices, and (i) Good Manufacturing Practices. Special controls may include special labeling requirements, mandatory performance standards and postmarket surveillance.

9.7 Performance Schedule, Marketing, and Projections. The anticipated schedule for the major Phase II tasks is shown in the chart on the following page, and it includes an aggressive testing and productizing emphasis to insure that stable products are being delivered as soon as practical.

There are over 13,000 MRI systems installed world-wide with annual MRI equipment sales of approximately $3B. The proposed rf coils would permit substantially reduced imaging time (hence, cost) and reduced patient distress for head imaging in most high-field MRI scanners above 1.5 T at relatively modest upgrade costs which would easily be recouped by MRI facilities. The initial product resulting from Phase II funding would be a 3T ^{1}H CP Head Coil, followed closely by a 3 T knee coil. Marketing of these products for research applications is expected to begin within eight months of the start of the Phase II, but it is unlikely that such sales will exceed $60K in the first year. Advertising and promotion would initially be limited to technical and vendor-exhibit presentations at technical conferences where we normally present our research products (ISMRM, ESMRMB, RSNA, and ENC). Following FDA approval, which is scheduled for about 18-19 months into the Phase II funding, wider marketing would begin.

As the FDA continues to approve higher fields for clinical head imaging (3T within the last 2 years,) MRI facilities will continue to upgrade their equipment for fields above 1.5T. Significant opportunity exists for the 2-4T head, knee, neck, and small-animal coils with the advantages of those we are developing. Market potential for the first year following the Phase II development should exceed $200K for these coils; and 40% annual growth should be achieved for the following ten years, bringing annual sales to ~$6M in ten years. Sales could begin to stabilize at that point.

Task Description	1 - 6	7 - 12	13 - 18	19 – 24
Evaluation of commercial EM software for MRI RF coils	X X X X			
Dev. of manufacturing process for head passive shims	X X			
Field testing of 3T ^{1}H CP Head Coil at HMC	X X X			
Write more flexible Pre- and Post-processor for *COILS*	X X	X X		
Detailed design, fabrication, eval., doc. of rev. ^{1}H Head Coil		X X X	X X	
Full-wave simulations of litz coils at HMC	X X X	X X X		
Simulations, design, and fabrication of ^{1}H CP 3 T knee coil	X X X			
Field testing of 3T ^{1}H CP Knee Coil at HMC	X X	X X		
Simulations, design, and fabrication of ^{1}H CP 200 MHz rat coil	X X			
Field testing of 200 MHz ^{1}H CP mouse/rat coil at Wash. Univ.	X X	X X X		
Simulations, design, and fabrication of ^{1}H/X 3 T head coil	X	X X X		
Field testing of 3T ^{1}H/X CP Head Coil at HMC		X	X X	
Simulations of novel coils – axial flux and Φ_E manipulation		X X X	X X X X	
Development of advanced Coupled TRL BP litzcage models		X X X X	X X X X	
Experiments on novel 17 cm volume coils at 300-500 MHz		X X	X X	
Obtain FDA approval of 3T ^{1}H CP Head Coil			X X X	X X
Obtain FDA approval of 3T ^{1}H CP Knee Coil			X	X X X
Simulations and detailed design of 3 T torso coil			X X	
Manufacture/construction of prototype 3 T torso coil			X X X	
Simulations, design, and fabrication of ^{1}H CP 500 MHz rat coil		X X X	X	
Field testing of 500 MHz ^{1}H CP mouse/rat coil at Wash. Univ.			X X	X X
Testing of 3T ^{1}H CP Torso Coil at HMC				X X X X
Improvements in torso coil and simulations				X X
Submit technical papers to appropriate journal		X		X
Submit Reports to NIH	X	X	X	X

9.7 Patent Status. Doty Scientific owns the pioneering patent on MRI RF litz coils (**6,060,882)**, which covers all types of both linear and CP MRI rf litz coils being considered. DSI also owns several other relevant patents, which are listed below.

F. D. Doty and James K. Wilcher, "Crescent Gradient Coils", 5,554,929 (1996).
F. D. Doty, "Non-dipolar NMR RF Lock Coil", 5,929,639 (1999).
F. D. Doty and Y. Yang, "HR MAS NMR Coils with Magic Angle Capacitors", 6,130,537, (2000).
F. David Doty, "Edge-wound RF Solenoid for NMR," 6,087,832, (2000).
F. D. Doty, "Low Inductance Transverse Litz Foil Coils", 6,060,882 (2000).
F. D. Doty, and George Entzminger, "Thermal Buffering of Cross-coils in High-power NMR Decoupling," 6,320,384 (2001).

Several of the developments that occurred during the Phase I are likely to result in patent applications during the Phase II. Among these are: "High-order Passive Shims for Head MRI," "A novel 4-point-drive circuit for CP MRI coils using 6 nλ/2 TRLs," and "A Five-ring CP Litzcage RF Coil for MRI." The passive shims are discussed in the Phase II proposal, section 4.7; and some of the basic aspects of the novel balancing network are discussed in section 4.8 and several earlier sections. The four-ring CP litzcage was discussed briefly in section 4.8, and the possible justification for a fifth ring (controlling the axial end flux) was discussed in section 4.5, but few details and experimental results were presented.

10. Similar Grant Applications, Proposals, or Awards

No prior, current, or pending support for the proposed work.

DSI has been awarded one Phase II Grant (DOE DE- FG02-98ER82565) in the past ten years for "Development of 1-10 W, 10 K Reverse Brayton Cycle Cryocoolers". PI: F. D. Doty. DOE Project officer: Carl Friesen, Argonne, IL. Awarded June 15, 1999. Funding ended June 15, 2001. No overlap.

A Phase I SBIR grant, R43 NS41127-01, for the development of an MRI head gradient coil, was awarded 5/01 from NIH. PI: F. D. Doty. No overlap.

A Phase I SBIR grant, 1 R43 RR16417-01, for the development of a 50 kHz ^{1}H NMR MAS probe for protein structure determination, was awarded 8/01. PI: F. D. Doty. No overlap.

A Phase I SBIR proposal, 1 R43 CA96155-01, was submitted 7/29/01 to NIH for the development of an MAS NMR probe with cryogenically cooled circuitry. No overlap.

There are no other current or pending proposals.